Available online at www.sciencedirect.com
SCIENCE DIRECT®
Journal of Sound and Vibration 289 (2006) 657–688
JOURNAL OF SOUND AND VIBRATION
www.elsevier.com/locate/jsvi

Dynamics of a 3dof torsional system with a dry friction controlled path

Chengwu Duan, Rajendra Singh*

Acoustics and Dynamics Laboratory, Department of Mechanical Engineering, The Center for Automotive Research, The Ohio State University, Columbus, OH 43210, USA

Received 14 July 2003; received in revised form 16 February 2005; accepted 16 February 2005
Available online 6 May 2005

Abstract

A three-degrees of freedom semi-definite torsional system representing an automotive driveline is studied in presence of a torque converter clutch that manifests itself as a dry friction path. An analytical procedure based on the linear system theory is proposed first to establish the stick-to-slip boundaries. Smoothened and discontinuous Coulomb friction formulations are then applied to the nonlinear system, and the differential governing equations are numerically solved given harmonic torque excitation and a mean load. Time domain histories illustrating dry friction-induced stick–slip motions are predicted for different saturation torques and system parameters. Approximate analytical solutions based on distinct states are also developed and successfully compared with numerical studies. Analysis shows that the conditioning factor associated with the smoothened friction model (hyperbolic tangent) must be carefully selected. Then nonlinear frequency responses are constructed from cyclic time histories and the stick–slip boundaries predictions (as yielded by the linear system theory) are confirmed. In particular, the effect of secondary inertia is analytically and numerically investigated. Results show that the secondary inertia has a significant influence on the dynamic response. A quasi-discontinuous oscillation is found with the conventional bi-linear friction model in which the secondary inertia is ignored. Finally, our methods are successfully compared with two benchmark analytical and experimental studies, as available in the literature on two-degrees of freedom translational systems.

*Corresponding author. Tel.: +1 614 292 9044; fax: +1 614 292 3163.
E-mail address: singh.3@osu.edu (R. Singh).

0022-460X/$ - see front matter © 2005 Elsevier Ltd. All rights reserved.
doi:10.1016/j.jsv.2005.02.029

Nomenclature

C	torsional viscous damping coefficient (N m s/rad)
f	dimensionless force
F	force (N)
I	torsional inertia (kg m^2)
K	torsional stiffness (N m/rad)
k	dimensionless stiffness
m	dimensionless mass
P	period (s)
p	dimensionless stiffness
r	dimensionless mass
t	time (s)
T	torque (N m)
V	relative velocity
Γ	test function (N m)
Δ	small quantity
δ	relative angular displacement (radian)
ζ	viscous damping ratio
θ	absolute angular displacement (rad)
μ	friction coefficient
ξ	normalized absolute displacement
ρ	dimensionless friction force amplitude
σ	conditioning factor
τ	integration time (s)
ϕ	phase (rad)
ψ	phase lag (rad)
Ω	angular speed (rad/s)
ω	excitation frequency (rad/s)
Im	test function (rad/s)^2
Re	decision function (N m)
y	normalized absolute displacement
φ	phase lag (rad)

Subscripts

1, 2, 3	inertial element indices
c	critical or transition
D	drag load
e	engine or equivalent
eq	equivalent
f	friction
k	kinetic
m	mean
n	natural frequency
max	maximum
min	minimum
p	fluctuating component or perturbation
s	static
sf	saturation

Superscripts

.	first derivative with respect to time
..	second derivative with respect to time

Operators

| |	absolute value
$\langle\rangle_t$	time-average operator
int( )	integer portion

Abbreviations

dof	degrees of freedom
sdof	single-degree of freedom system
2dof/3dof	two/three-degrees of freedom system
max	maximum value
min	minimum value
rms	root-mean-square

1. Introduction

Dry friction elements are commonly found in many mechanical and structural systems. For example, consider the automotive torque converter clutch (TCC) sub-system that consists of a fluid torque converter and in parallel a mechanical dry friction clutch as shown in Fig. 1. When

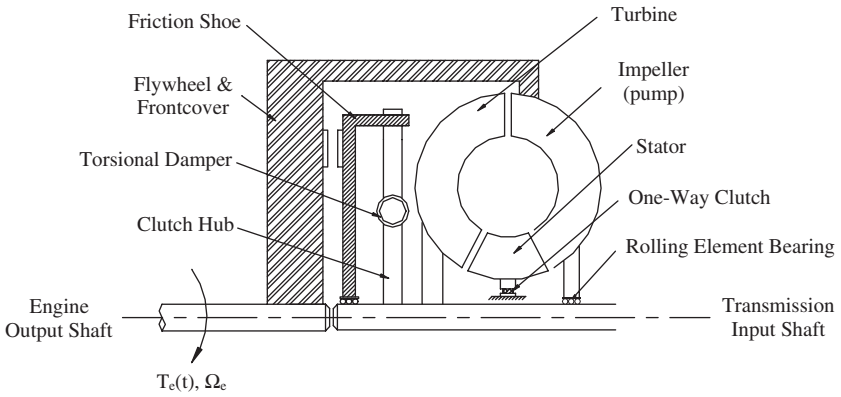

Fig. 1. Schematic of a typical automotive torque converter and dry friction clutch (TCC).

the engine speed Ω_e is low, the dry friction clutch is fully disengaged and only the fluid torque converter path is operational. The pump drives the turbine with a torque generated by a change in the momentum of the fluid. Torque amplification is allowed and a smooth shift or transition is allowed [1]. At a higher speed, the mechanical clutch is fully engaged and the fluid path is no longer in effect. Under this condition, the transmission is directly driven by the engine. The energy dissipated within the torque converter is minimized to enhance the fuel efficiency. Over the mid-speed range, the TCC is partially engaged and both the dry friction clutch and the fluid torque converter transmit torque [2,3]. The TCC is designed to transmit very high torque loads and to suppress a large slip between engine and transmission to avoid overheating. However, the stick–slip phenomenon often takes place within the TCC as a consequence of significant torque pulsations from the engine. The resulting stick–slip could excite several vibration problems in the driveline system, thereby reducing the vehicle ride quality. To study the dynamic effects of stick–slip within a driveline system with TCC, we will study the nonlinear dynamic characteristics of a three-degrees of freedom (3dof) semi-definite torsional system with a dry friction controlled path.

2. Literature review and research issues

2.1. Typical dry friction models

Several dry friction formulations have been proposed based on the classical (discontinuous) Coulomb model that is illustrated in Fig. 2a. For instance, Karnopp [4] developed a stick–slip friction law in which the friction force or torque T_f is defined as a function of the relative velocity $\dot{\delta}$. A small region of velocity $\pm\Delta\dot{\delta}$ is defined as the stick stage in Fig. 2b. Beyond this, the friction interface is considered to be in the slip stage. Following Iwan's bi-linear hysteresis formulation [5], Menq et al. [6] proposed a modified micro-slip model by modeling the friction interface in terms of an elasto-plastic shear layer. Three different states are defined in Fig. 2c: purely elastic, partial slip and total slip. When the relative displacement reaches a certain value δ_e, the deformation between

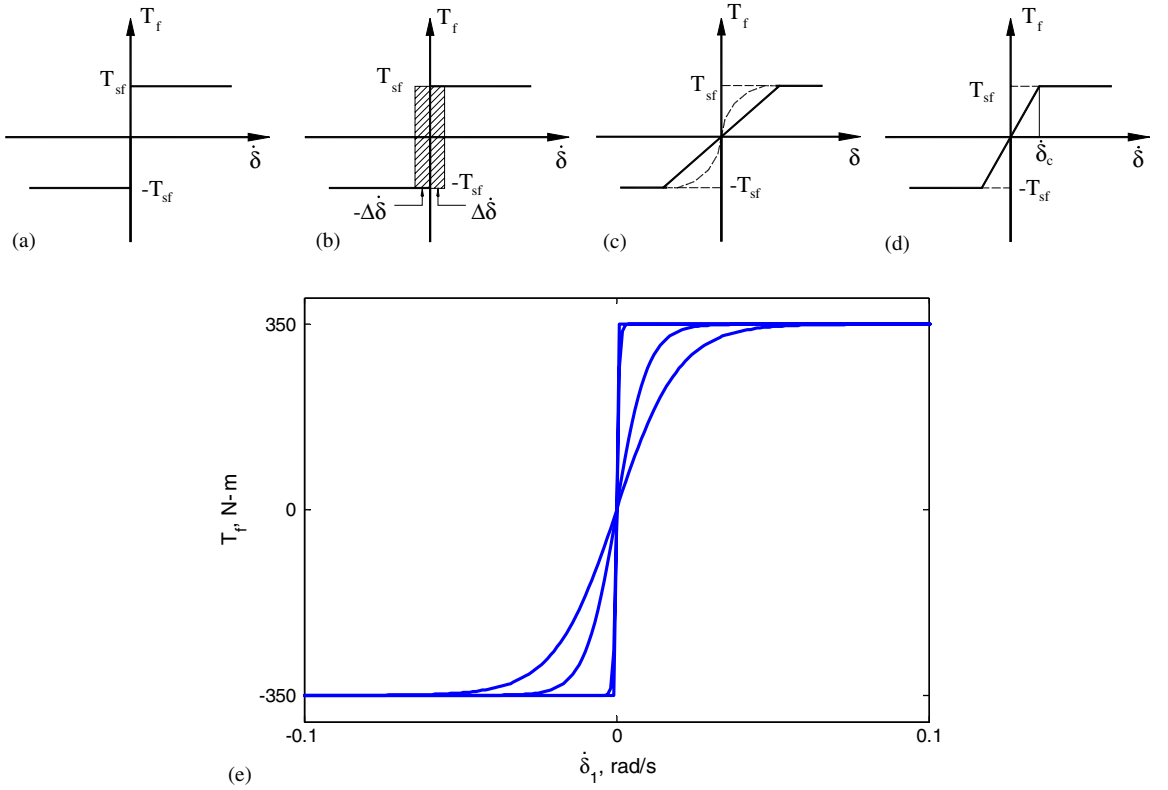

Fig. 2. Selected dry friction formulations: (a) classical (discontinuous) Coulomb model; (b) Karnopp model [4]; (c) Menq et al.'s models [6]: - - - - - -, elastic bar on rigid base; ——, elastic bar with an elastoplastic shear layer on a rigid base; (d) model by Imamura et al. [7]; (e) smoothened friction formulation $T_f(\dot{\delta})$ of our study with a variable conditioning factor σ and with saturation torque $T_{sf} = 350\,\mathrm{N\,m}$: Key for (e): – - – - –, $\sigma = 50$; ——, $\sigma = 10^2$; – – – – – –, $\sigma = 10^3$; ——, $\sigma = 10^4$.

interfaces becomes plastic and the gross slip takes place. Consequently, the friction force reaches a saturation value T_{sf}. This model could further consider unloading and reloading cases, in which the material memory effect is taken into account. Imamura et al. [7] developed a new friction torque model as shown in Fig. 2d with an application to automotive clutch system. Unlike the bi-linear hysteresis model in which δ_c is defined at the kinetic transition point, a critical velocity $\dot{\delta}_c$ is defined here. The friction torque varies linearly with $\dot{\delta}$ within the critical bounds $\pm\dot{\delta}_c$. Finally, other models can be derived from the aforementioned formulations by selecting the static friction coefficient μ_s or kinetic friction coefficient μ_k, or by assuming a specific $\mu_k(\dot{\delta})$ relation.

2.2. Solution methods

Several analytical or computational methods have been applied to solve the dry friction problems. Den Hartog [8] initiated research in this area by analytically solving the forced vibration problem of a single-degree of freedom (sdof) system with Coulomb friction. He

determined an equivalent viscous damping value under pure slipping case and then found the time history with a limit of no more than 2 stops. With the assumption of periodic and aperiodic motions, Pratt and Williams [9] extended Den Hartog's work and calculated the system response with multi-lockups by using a shooting method. Also, they calculated the equivalent viscous damping on a time-averaged basis. Shaw [10] extended the previous work by including different static μ_s and kinetic μ_k coefficients; he also conducted bifurcation and stability analyses. Menq et al. [11,12] and Wang et al. [13,14] used a multi-term harmonic balance method to find the dynamic response of a bi-linear hysteresis problem. Ferri and Heck [15] and Ferri [16] solved a two-degrees of freedom (2dof) system by using a modified singular perturbation method. In their method, the system order is reduced to eliminate the numerical stiffness problem. Van De Vrande et al. [17] solved a dry friction-induced stick–slip problem by smoothening the discontinuous dry friction force with an arc-tangent function and then studied the autonomous systems from the phase plane viewpoint. Leine et al. [18] proposed an alternate friction model using a concept similar to Karnopp's formulation. Berger et al. [19] proposed a mixed differential–algebraic equation approach that uses differential equations to describe the slipping dynamics and algebraic equations to model the interfacial sticking. In their method, a zeroth-order optimization algorithm is proposed to detect the transition from stick to slip.

2.3. Some unresolved problems

Many investigators have focused on sdof systems with application to the dry friction damper. In such systems, the friction force is relatively small compared to the excitation force amplitude and the dry friction damper is used mainly to absorb or dampen forced vibration [8–16,20]. Further, much research has focused on the description of friction interfacial regimes [4–6]. Nonetheless, dry friction elements invariably exist in many real-life mechanical systems and rather than dissipating energy, the dry friction path acts as a key energy transmitting element. For instance, the friction capacity of the dry friction clutch (TCC) could be as high as 450 N m, which is comparable to the peak value of the dynamic torque generated by the engine [7]. In this case, TCC cannot be considered as a purely frictional vibration damper. Instead, the friction torque from TCC becomes a dominant excitation to the subsequent torsional driveline sub-system (downstream of TCC) consisting of gearbox, propeller shaft, differential, axle and wheels. Consequently, the dynamics of the driveline system is significantly determined by the localized stick–slip motions within TCC. However, the scientific literature on this effect of dry friction on system dynamics is very limited. For example, some researchers have focused on a bi-linear hysteresis problem by assuming a massless link between the spring and Coulomb friction elements [5,6,11–14]. However, that is not always true for some physical systems since a small secondary lumped inertial element could exist. Effect of such a secondary inertia on the system dynamics is still not well understood though Ferri and Heck [15] briefly mentioned the significance on a secondary mass in the context of a dry friction damper. Recently, Berger and Krousgrill [20] examined the role of a secondary mass in dissipating energy and evaluated its influence on the kinetic state of the damper. They found that the non-zero secondary mass damper would substantially attenuate the resonant response when compared with a massless bi-linear system.

3. Problem formulation

3.1. Torsional system with dry friction controlled path

The driveline system can be reasonably represented by a 3dof semi-definite system with focus on the TCC sub-system. This is conceptually similar to the manual transmission formulation employed by Padmanabhan and Singh [21] to study gear rattle and to the automatic transmission model utilized by Yamada and Ando [22] to examine clutch judder. As shown in Fig. 3, I_1 represents the combined torsional inertia of flywheel, front cover and impeller, I_2 is the inertia of friction shoe assembly and I_3 is the reflected torsional inertia of the rest of the driveline system. The governing equations for this 3dof semi-definite system with a nonlinear dry friction path as given by T_f are

$$I_1\ddot{\theta}_1 + C(\dot{\theta}_1)(\dot{\theta}_1 - \dot{\theta}_3) + T_f(\delta_1, \dot{\delta}_1) = T_e(t), \tag{1}$$

$$I_2\ddot{\theta}_2 + K(\theta_2 - \theta_3) - T_f(\delta_1, \dot{\delta}_1) = 0, \tag{2}$$

$$I_3\ddot{\theta}_3 - C(\dot{\theta}_1)(\dot{\theta}_1 - \dot{\theta}_3) - K(\theta_2 - \theta_3) = -T_D(t), \tag{3}$$

where θ_1, θ_2 and θ_3 are absolute angular displacements, $C(\dot{\theta}_1)$ is the engine speed-dependent viscous damping term which represents the fluid path, K is the linear torsional stiffness, $T_e(t)$ is the engine torque (including mean and dynamic terms) and $T_D(t)$ is the drag load as experienced by the driveline. Further, in Eq. (1), $T_f(\delta_1, \dot{\delta}_1)$ is a function of the relative displacement $\delta_1 = \theta_1 - \theta_2$ and relative velocity $\dot{\delta}_1 = \dot{\theta}_1 - \dot{\theta}_2$ across the dry friction interface. When the relative motions are of interest, the system can be further reduced to the following 2dof definite system, where $\delta_2 = \theta_2 - \theta_3$ and $\dot{\delta}_2 = \dot{\theta}_2 - \dot{\theta}_3$:

$$I_2\ddot{\delta}_1 + C(\dot{\theta}_1)\frac{I_2}{I_1}(\dot{\delta}_1 + \dot{\delta}_2) - K\delta_2 + \frac{I_1 + I_2}{I_1}\,T_f(\delta_1, \dot{\delta}_1) = \frac{I_2}{I_1}\,T_e(t), \tag{4}$$

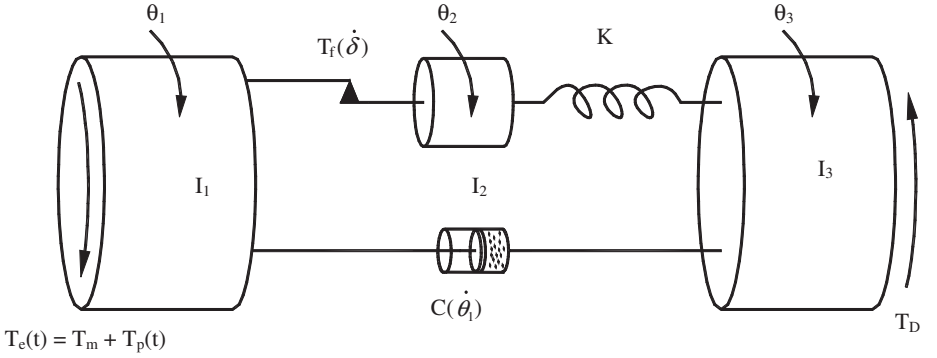

Fig. 3. Physical example: 3dof semi-definite torsional model of an automotive driveline system. Here, $T_f(\dot{\delta})$ represents a dry friction path.

Table 1
Values of parameter and excitation amplitude used for simulating the system of Fig. 3

Parameters and excitation	Value(s)
Torsional inertias (kg m^2)	$I_1 = 0.20$, $I_2 = 0.02$, $I_3 = 6.6$
Torsional viscous damping (N m rad/s)	$C = 1.0$
Torsional stiffness (N m/rad)	$K = 1010$
Saturation friction torque (N m)	$T_{sf} = 350$
Torque excitation amplitude (N m)	$T_m = 100$, $T_p = 250$

$$I_2\ddot{\delta}_2 + C(\dot{\theta}_1)\frac{I_2}{I_3}(\dot{\delta}_1 + \dot{\delta}_2) + \frac{I_2 + I_3}{I_3}K\delta_2 - T_f(\delta_1, \dot{\delta}_1) = \frac{I_2}{I_3}T_D(t). \tag{5}$$

Table 1 lists typical values of parameters and excitation used for simulation studies.

3.2. Scope, assumptions and objectives

The engine torque $T_e(t)$ is composed of mean $T_m = \langle T_e \rangle_t$ and pulsating $T_p(t)$ components, where $\langle\,\rangle_t$ is the time-averaged operator. Using the Fourier series expansion, express it as

$$T_e(t) = T_m + \sum_n T_{pn}\cos(\omega_{pn}t + \phi_{pn}),$$

where n is the harmonic order of the firing sequence, $\omega_{pn} = (N_e/2)n\Omega_e$, N_e is the number of engine cylinders [23,24], T_{pn} is the amplitude for the nth harmonic and ϕ_n is the associated phase lag. In this article, only the fundamental term ($n = 1$) is considered for the sake of simplicity and the phase angle is assumed to be zero. The drag load $T_D(t)$ consists of wheel rolling resistance and aerodynamic drag. It is further assumed that the vehicle speed is constant and the vehicle drag and the mean engine load are balanced, $T_m = T_D$.

Even when the TCC is partially engaged, most of the torque is transmitted by the mechanical path [3]. Thus, the driveline system dynamics is assumed to be mostly affected by the mechanical stick–slip motions. In this case, the fluid path term $C(\dot{\theta}_1)$ is further approximated by a linear viscous damping C. In a real system, C could be around 1.0 N m s/rad [1]. Further, under a high normal load, the shear stiffness of the friction interface is assumed to be very large. Consequently, the discontinuous Coulomb model is used and $\mu_s = \mu_k$ is assumed. The normal force on the friction interface remains unchanged and the friction torque T_f capacity is fixed accordingly.

Given a nonlinear dry friction problem, time domain integration methods are usually employed [4,8,9,18]. However, the solution process consumes significant time and yet the resulting time history at a certain frequency (under a given mean load) does not provide an overall characterization of the nonlinear system from the design standpoint. Further, actual time histories may not be important for some engineering applications. Consequently, steady-state frequency response characteristics must be constructed to provide better and easy-to-follow dynamic design guidelines [25]. This article will accordingly also examine the nonlinear frequency response of the driveline system since it is rarely discussed in the dry friction literature [21,25].

Finally, for any nonlinear system, super or sub-harmonic responses, multi-valued equilibrium points, quasi-periodic or chaotic responses may be present. However, such nonlinear issues will be addressed in a future article.

The chief objective of this study is to investigate the nonlinear dynamics of the 3dof system representing the torsional driveline system subject to the localized stick–slip motions of the dry friction path. In particular, the effect of the secondary inertia (I_2) that represents the friction shoe assembly here is studied and compared with the conventional bi-linear system. Two solution methods, namely the smoothened friction model and discontinuous Coulomb model, are employed. The effect of the conditioning factor σ (as defined later) on system dynamics will be studied. Approximate analytical solutions, based on assumed states (such as pure stick, positive or negative slip) will also be developed and compared with computational solutions. Time histories are presented to assist the frequency domain analyses. The stick-to-slip boundaries will be first determined based on the linear system theory and then examined using the nonlinear models. The effect of the friction torque amplitude (a path parameter) is of particular interest. Further, the effect of secondary inertia will be carefully examined using both numerical and approximate analytical solutions. Finally, our models are applied to two benchmark analytical and experimental studies [15,26] for the sake of validation.

4. Computation of stick-to-slip boundaries based on linear system models

In the case of a high friction torque T_{sf}, a closer observation would find that the friction interface is under purely the stick condition over some frequencies. A simple linear system analysis is conducted to find this frequency regime. The schematic of a system under the pure stick condition is shown in Fig. 4a. In this case, I_1 and I_2 move together as a single rigid body and the 3dof semi-definite system is reduced to a 2dof semi-definite system with equations as

$$(I_1 + I_2)\ddot{\theta}_1 + C(\dot{\theta}_1 - \dot{\theta}_3) + K(\theta_1 - \theta_3) = T_e, \tag{6}$$

$$I_3\ddot{\theta}_3 - C(\dot{\theta}_1 - \dot{\theta}_3) - K(\theta_1 - \theta_3) = -T_D. \tag{7}$$

Reducing this linear system further into sdof definite system, the governing equation is given as follows where the sinusoidal excitation (at ω with amplitude T_{eq}) under a mean load T_m is applied:

$$I_{eq}\ddot{\delta} + C\dot{\delta} + K\delta = T_m + T_{eq}\sin(\omega t), \tag{8}$$

where $\delta = \theta_1 - \theta_3 = \theta_2 - \theta_3$, $I_{eq} = I_3(I_1 + I_2)/(I_1 + I_2 + I_3)$ and $T_{eq} = T_p I_3/(I_1 + I_2 + I_3)$. The analytical solution for the steady-state oscillatory motions (δ and $\dot{\delta}$) is as follows, where $\psi = \tan^{-1}[C\omega/(K - I_{eq}\omega^2)]$ is the phase lag.

$$\delta(t) = \frac{T_m}{K} + \frac{T_{eq}}{\sqrt{(K - I_{eq}\omega^2)^2 + (C\omega)^2}}\sin(\omega t - \psi), \tag{9}$$

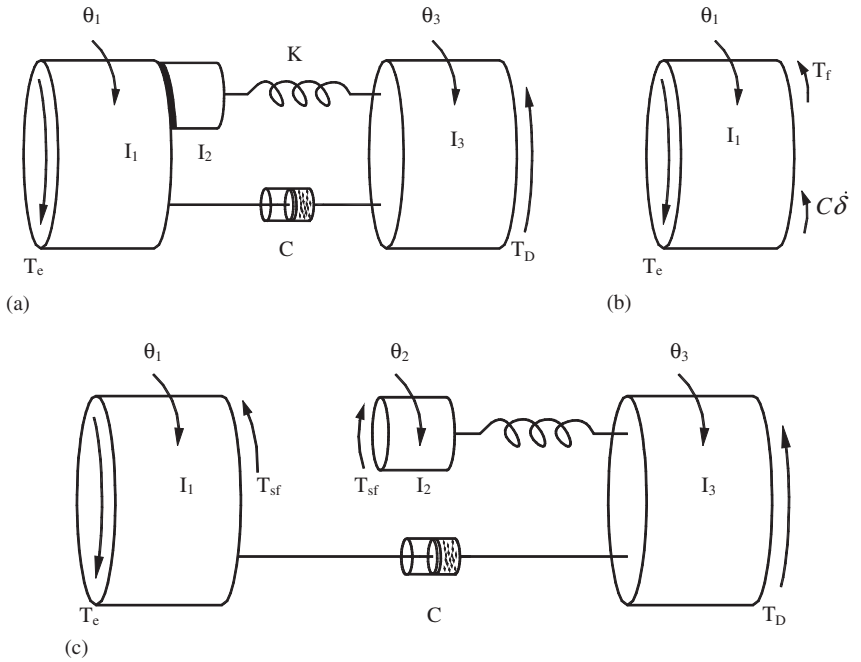

Fig. 4. Resulting torsional systems under different conditions: (a) pure stick condition; (b) free body diagram for I_1 under pure stick conditions and (c) positive slip condition.

$$\dot{\delta}(t) = \frac{T_{\text{eq}}\omega}{\sqrt{(K - I_{\text{eq}}\omega^2)^2 + (C\omega)^2}}\cos(\omega t - \psi). \tag{10}$$

As seen from the free body diagram of Fig. 4b, the following relationship holds under the pure stick condition:

$$T_e(t) - I_1\ddot{\theta}_1(t) - C\dot{\delta}(t) = T_f(t). \tag{11}$$

Then the transition condition from stick to slip is

$$|T_e(t) - I_1\ddot{\theta}_1(t) - C\dot{\delta}(t)| > T_{\text{sf}}. \tag{12}$$

From Eq. (6), substitute $\ddot{\theta}_1(t) = [T_e(t) - C\dot{\delta}(t) - K\delta(t)]/(I_1 + I_2)$ into Eq. (12) to find the breakaway condition as

$$\left|\frac{I_2}{I_1 + I_2}\,T_e(t) - \frac{I_2}{I_1 + I_2}\,C\dot{\delta}(t) + \frac{I_1}{I_1 + I_2}\,K\delta(t)\right| > T_{\text{sf}}. \tag{13}$$

As evident from this analysis, the stick-to-slip boundary is determined by system parameters that are summarized in Table 1. As shown in Fig. 5a, the upper threshold frequency drops as the secondary inertia I_2 is increased. A pure stick regime is found at the lower-frequency range. Depending on the friction saturation torque, the pure stick regime exists at lower frequencies as shown in Fig. 5b. The excitation amplitude yields an opposite trend in Fig. 5c where the pure stick

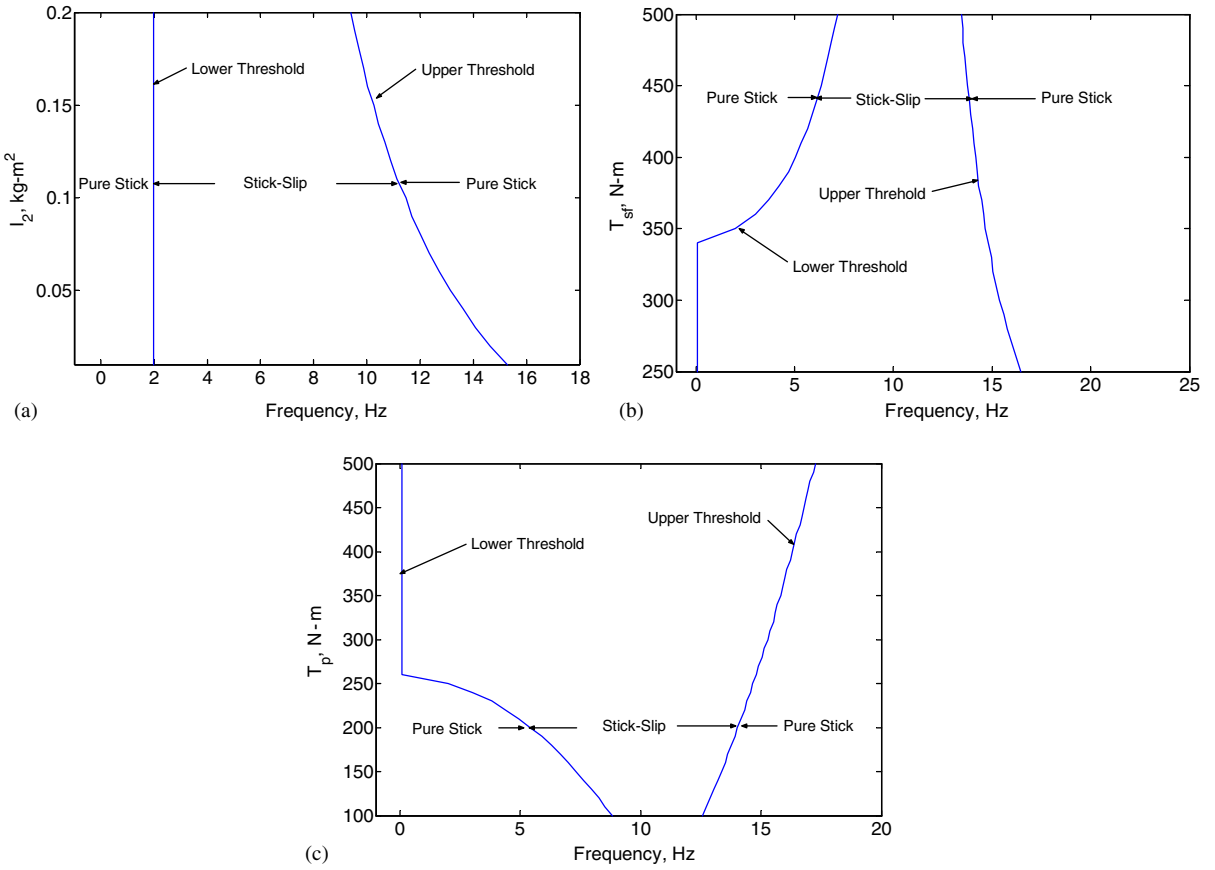

Fig. 5. Stick–slip boundaries based on linear system analysis: (a) variation with respect to I_2; (b) variation with respect to T_{sf} and (c) variation with respect to excitation amplitude of T_p.

regime occurs at a lower excitation torque. This analysis can also be applied to other physical systems where a dry friction element is present. The stick–slip transition could be quickly located and the entire simulation process would become more time efficient.

5. Analytical and numerical solutions to nonlinear path formulation

5.1. Smoothened friction torque model

The classical Coulomb model is $T_f(\dot{\delta})$ a non-smooth function since it is discontinuous with respect to $\dot{\delta}$ and a singularity exists at $\dot{\delta} = 0$. For this reason, the direct numerical integration scheme cannot be applied. To overcome this difficulty, a smoothening procedure could be used to condition the abrupt transitions. Ways to smoothen a discontinuous function using arc-tangent, hyperbolic tangent, hyperbolic-cosine or quintic spline functions have been proposed by Kim

et al. [27] with an application to the clearance nonlinearity. In their study, the hyperbolic tangent and arc-tangent function were preferred because of their applicability to both direct time domain integration and semi-analytical (such as the multi-term harmonic balance) methods. The smoothened friction model can be described by a continuous but still a strongly nonlinear function, as shown below, in terms of the hyperbolic tangent function. The resulting nonlinear friction torque is given by

$$T_f = T_{\mathrm{sf}} \tanh(\sigma\dot{\delta}_1), \tag{14}$$

where T_{sf} is the saturation torque (torque at the kinetic state) and σ is the conditioning factor that control the abruptness of the transition as illustrated in Fig. 2e. The higher the value of σ is, the more abrupt the transition is. An extremely high value of σ would yield a profile that would resemble the classical Coulomb model. Further, the smoothened friction model of Eq. (14) yields a unique T_f corresponding to a certain value of $\dot{\delta}_1$. Thus the friction torque would be viewed as an "active torque" with $\dot{\delta}_1$. The smoothening procedure is used mainly to facilitate the direct numerical integration scheme as T_f becomes a smooth function of $\dot{\delta}_1$ over the entire vector space.

When the smoothened friction model is used, the nonlinear friction torque becomes an explicit nonlinear function of $\dot{\delta}$. Using Eqs. (4)–(5), the governing equations can be rewritten as

$$I_2\ddot{\delta}_1 + C\frac{I_2}{I_1}(\dot{\delta}_1 + \dot{\delta}_2) - K\delta_2 + \frac{I_1 + I_2}{I_1} T_{\mathrm{sf}} \tanh(\sigma\dot{\delta}_1) = \frac{I_2}{I_1} T_e(t) = \frac{I_2}{I_1}(T_m + T_p \sin\omega t), \tag{15}$$

$$I_2\ddot{\delta}_2 + C\frac{I_2}{I_3}(\dot{\delta}_1 + \dot{\delta}_2) + \frac{I_2 + I_3}{I_3} K\delta_2 - T_{\mathrm{sf}} \tanh(\sigma\dot{\delta}_1) = \frac{I_2}{I_3} T_D. \tag{16}$$

Since there is no spring in parallel with the dry friction element, δ_1 does not appear in the system equations. An explicit Runge–Kutta method of order 5(4) with a step size control due to Dormand and Prince [28] can be applied directly to this system to find the resulting response.

5.2. Analytical solution for the positive slip state

Unlike the smoothened friction model, the discontinuous friction torque, as given below, treats T_f as a "passive torque" that is determined by external excitation and system response. Here, T_f can assume any value between $-T_{\mathrm{sf}}$ and T_{sf} at $\dot{\delta}_1 = 0$:

$$T_f = \begin{cases} T_{\mathrm{sf}}, & \dot{\delta}_1 > 0, \\ [-T_{\mathrm{sf}}\ T_{\mathrm{sf}}], & \dot{\delta}_1 = 0, \\ -T_{\mathrm{sf}}, & \dot{\delta}_1 < 0. \end{cases} \tag{17}$$

Thus the friction torque behaves in a piecewise linear manner. Three different dynamic states (positive slip, negative slip and pure stick) are defined depending on the frictional interfacial condition. In each state, an effective linear model is considered. First, examine the positive slip state, $\dot{\delta}_1 = \dot{\theta}_1 - \dot{\theta}_2 > 0$. The friction torque is constant and equal to T_{sf} as shown in Fig. 4c. The governing equations for this state are

$$I_2\ddot{\delta}_1 + C\frac{I_2}{I_1}(\dot{\delta}_1 + \dot{\delta}_2) - K\delta_2 + \frac{I_1 + I_2}{I_1} T_{\mathrm{sf}} = \frac{I_2}{I_1} T_e(t), \tag{18}$$

$$I_2\ddot{\delta}_2 + C\frac{I_2}{I_3}(\dot{\delta}_1 + \dot{\delta}_2) + \frac{I_2 + I_3}{I_3}K\delta_2 - T_{sf} = \frac{I_2}{I_3}T_D. \tag{19}$$

As seen from Table 1, $I_3 \gg I_2$ for a typical automotive driveline system. For this reason, Eq. (19) can be approximated by discarding the viscous damping torque associated with $\dot{\delta}_1$. Further, one could decouple $\dot{\delta}_1$ and δ_2 by dropping the appropriate terms in Eqs. (18) and (19). However, we must keep the $C(I_2/I_1)\dot{\delta}_2$ term since the viscous damping is needed to avoid the unbound solution due to resonance. Simplify Eq. (19) to yield the following:

$$I_2\ddot{\delta}_2 + C\frac{I_2}{I_3}\dot{\delta}_2 + \frac{I_2 + I_3}{I_3}K\delta_2 - T_{sf} = \frac{I_2}{I_3}T_D. \tag{20}$$

The solution for $\delta_2(t)$ is first obtained where $\beta = I_2/I_3$ and t_c is the transition time from the pure stick to the positive slip.

$$\delta_2(t) = \frac{\beta T_D + T_{sf}}{(1+\beta)K} + e^{-\lambda(t-t_c)}\{p_1\cos(\omega_d(t-t_c)) + p_2\sin(\omega_d(t-t_c))\}, \tag{21a}$$

$$\lambda = \frac{-C\beta}{2I_2}, \quad \omega_d = \frac{\sqrt{4I_2(1+\beta)K - C^2\beta^2}}{2I_2}. \tag{21b,c}$$

Assuming the initial values

$$\delta_2|_{t=t_c} = \Lambda_2, \quad \dot{\delta}_2|_{t=t_c} = V_2. \tag{22a,b}$$

The coefficients p_1 and p_2 are found as shown below.

$$p_1 = \Lambda_2 - \frac{\beta T_D + T_{sf}}{(1+\beta)K}, \quad p_2 = \frac{V_2 + \lambda P_1}{\omega_d}. \tag{23a,b}$$

Rewrite Eq. (18) in the following form where $\alpha = I_2/I_1$,

$$I_2\ddot{\delta}_1 + C\alpha\dot{\delta}_1 = \alpha T_e(t) - C\alpha\dot{\delta}_2 + K\delta_2 - (1+\alpha)T_{sf}. \tag{24}$$

Note that the right-hand side of Eq. (24) can be viewed as an equivalent excitation to a first-order linear system with a time constant $I_2/C\alpha = 1/\xi$. We obtain the solution for $\dot{\delta}_1(t)$ in the following torque functional form:

$$\dot{\delta}_1(t) = A_0 + A_1 e^{-\xi(t-t_c)} + \left\{\begin{array}{l} A_{21}\cos(\omega(t-t_c)) \\ + A_{22}\sin(\omega(t-t_c)) \end{array}\right\} + \left\{\begin{array}{l} A_{31}\cos(\omega_d(t-t_c)) \\ + A_{32}\sin(\omega_d(t-t_c)) \end{array}\right\} + A_4(t-t_c). \tag{25}$$

The coefficients ($A_0, A_1, A_{21}, A_{22}, A_{31}, A_{32}$ and A_4) can be obtained by satisfying the initial conditions $\delta_1|_{t=t_c} = \Lambda_1$ and $\dot{\delta}_1|_{t=t_c} = 0$. Although the exact expressions for the coefficients are not displayed here, Eq. (25) shows the oscillations occur with ω and ω_d in addition to a bias term (A_0), an exponentially decaying term, and a linear ramp.

5.3. Analytical solution for the negative slip state

Next, the equations for the negative slip state in which $\dot{\delta}_1 = \dot{\theta}_1 - \dot{\theta}_2 < 0$ and $T_f = -T_{sf}$ are given as follows. In Fig. 4c, the direction of T_{sf} must be reversed to illustrate this case.

$$I_2\ddot{\delta}_1 + C\frac{I_2}{I_1}(\dot{\delta}_1 + \dot{\delta}_2) - K\delta_2 - \frac{I_1 + I_2}{I_1}T_{\text{sf}} = \frac{I_2}{I_1}T_e(t), \tag{26}$$

$$I_2\ddot{\delta}_2 + C\frac{I_2}{I_3}(\dot{\delta}_1 + \dot{\delta}_2) + \frac{I_2 + I_3}{I_3}K\delta_2 + T_{\text{sf}} = \frac{I_2}{I_3}T_D. \tag{27}$$

The analytical solutions for this state can be obtained in a manner similar to those reported for the positive slip state in Section 5.2.

5.4. Analytical solution for the pure stick state

Finally, consider the pure stick condition. Now, I_1 and I_2 move as a single inertial body and the 3dof system is essentially reduced to a 2dof semi-definite system or a sdof definite system as shown in Fig. 4a. The governing equation is given by Eq. (8) as defined in Section 4. In this state, $\dot{\delta}_1 = 0$ and δ_1 remains constant and equal to the one from the end of previous state. The solution for $\delta_2(t)$ can be obtained by solving Eq. (8) as follows where $\gamma = C/2I_{\text{eq}}$. Assuming that the transition time from the positive or negative slip to the pure stick state is t_d, we again express it in a functional form where B_{11} and B_{12} are coefficients that are determined by the initial conditions. Like Eq. (25), observe a bias term (T_m/K) and an exponentially decaying term. But oscillations occur only with frequency ω.

$$\delta_2(t) = \mathrm{e}^{-\gamma(t-t_d)}\left\{\begin{array}{l} B_{11}\cos(\omega_s(t-t_d)) \\ +B_{12}\sin(\omega_s(t-t_d)) \end{array}\right\} + \frac{T_m}{K} + \frac{T_{\text{eq}}}{\sqrt{(K - I_{\text{eq}}\omega^2)^2 + (C\omega)^2}}\sin(\omega(t-t_d) - \psi). \tag{28}$$

5.5. Numerical solution of the discontinuous friction torque model

As presented in the previous sections, each state can be analytically solved and then the entire solution could be assembled. Alternatively, the equations can be solved by a fifth fourth-order Runge–Kutta integration algorithm. Test conditions and functions, however, must be defined at each state. At each integration step, the test function is checked. For instance when system undergoes positive or negative slip, the test function is defined as $\text{Im}(\tau_i) = \dot{\delta}_1(\tau_i)\dot{\delta}_1(\tau_{i+1})$, which is the product of the relative velocities of two successive integration steps. Whenever $\text{Im}(\tau_i)$ becomes negative, a possible transition to the stick state is detected and the program automatically finds the exact transition point within a pre-specified precision. A bi-section root finding algorithm is used; although this method may not be the most efficient algorithm, yet it is found very reliable by Gear and Osterby [29]. With a specified tolerance 10^{-6}, our code usually finds the exact point within 5–10 iterations. A test function for the stick state is defined as $\Gamma(\tau)$, which is actually the instantaneous interfacial friction torque. From Eq. (15), $\Gamma(\tau)$ is given by

$$\Gamma(\tau) = \frac{I_2}{I_1 + I_2}T_e(\tau) - \frac{I_2}{I_1 + I_2}C\dot{\delta}_2(\tau) + \frac{I_1}{I_1 + I_2}K\delta_2(\tau). \tag{29}$$

Whenever $|\Gamma(\tau)|$ is greater than T_{sf}, a possible transition from stick to slip is detected. Once the exact transition points are calculated, the subsequent state is determined by a decision function $\text{Re}(\tau)$ that is numerically identical to $\Gamma(\tau)$. The detailed state to state transition process is

Table 2
State-to-state transition for the nonlinear formulation of Fig. 3 with discontinuous Coulomb friction model

Previous state	Transition condition	Test function	Future state	δ_1 and $\dot{\delta}_1$
Positive slip	$\mathrm{Im}(\tau)<0$	$\lvert\mathrm{Re}(\tau)\rvert \leqslant T_{sf}$	Pure stick	$\delta_1=\delta_1^*;\quad \dot{\delta}_1=0$
		$\lvert\mathrm{Re}(\tau)\rvert > T_{sf}$	Negative slip	$\mathrm{sgn}(\dot{\delta}_1(\tau+0))=\mathrm{sgn}(f(\tau-0))$
Pure stick	$\lvert\Gamma(\tau)\rvert > T_{sf}$	$\mathrm{Re}(\tau) > T_{sf}$	Positive slip	$\mathrm{sgn}(\dot{\delta}_1(\tau+0))=\mathrm{sgn}(f(\tau-0))$
		$\mathrm{Re}(\tau) < -T_{sf}$	Negative slip	$\mathrm{sgn}(\dot{\delta}_1(\tau+0))=\mathrm{sgn}(f(\tau-0))$
Negative slip	$\mathrm{Im}(\tau)<0$	$\lvert\mathrm{Re}(\tau)\rvert > T_{sf}$	Positive slip	$\mathrm{sgn}(\dot{\delta}_1(\tau+0))=\mathrm{sgn}(f(\tau-0))$
		$\lvert\mathrm{Re}(\tau)\rvert \leqslant T_{sf}$	Pure stick	$\delta_1=\delta_1^*;\quad \dot{\delta}_1=0$

illustrated in Table 2. The sgn function used here is the conventional triple-valued signum function:

$$\mathrm{sgn}(\dot{\delta}_1)=\begin{cases}1, & \dot{\delta}_1>0,\\ 0, & \dot{\delta}_1=0,\\ -1, & \dot{\delta}_1<0.\end{cases} \tag{30}$$

Note that δ_1^* in Table 2 is the value of δ_1 at the end of previous positive or negative slip state and as discussed earlier, δ_1 remains this value during the subsequent pure stick state. In our simulation, the values of $\delta_1, \dot{\delta}_1, \delta_2$ and $\dot{\delta}_2$ at the end of a certain state provide the initial conditions for the next state. Finally, the solutions for all states are assembled.

5.6. *Effect of conditioning factor* σ

In the smoothened friction model of Eq. (14), the singularity at $\dot{\delta}=0$ of the classical Coulomb model is eliminated. However, this smoothening process brings an artificial uncertainty to the system since it is virtually impossible to determine the precise value of σ without a significant knowledge of its dynamics. From the standpoint of the rate of change of the friction torque at $\dot{\delta}=0$, the proposed procedure replaces the impulse function (with the discontinuous model) with the following finite derivative:

$$\frac{\mathrm{d}T_f}{\mathrm{d}\dot{\delta}}=T_{sf}\sigma[1-\tanh^2(\sigma\dot{\delta})]. \tag{31}$$

The maximum amplitude, $T_{sf}\sigma$, can now be taken as an indicator of its abruptness. As seen from Eq. (31), even for the same σ value, the abruptness of $T_f(\dot{\delta})$ profile would vary from system to system because of the saturation friction torque T_{sf}. Moreover, σ controls the integration speed. For example, a lower σ value gives a smoother torque curve and faster convergence is achieved in numerical integration. Conversely, a higher σ value can produce a Coulomb-like $T_f(\dot{\delta})$ curve. But too abrupt transition(s) would ill-condition the differential equations [30], and thereby

introducing numerical stiffness issues. Illustrative results are given in Figs. 6 and 7. When σ is 100, the calculated system response is almost identical to the one found with the discontinuous model. When σ is low such as 0.5, no pure stick regime is found in $\dot{\delta}_1(t)$ of Fig. 6. The friction torque undergoes a relatively smooth transition but the calculated response of $\delta_2(t)$ shows some

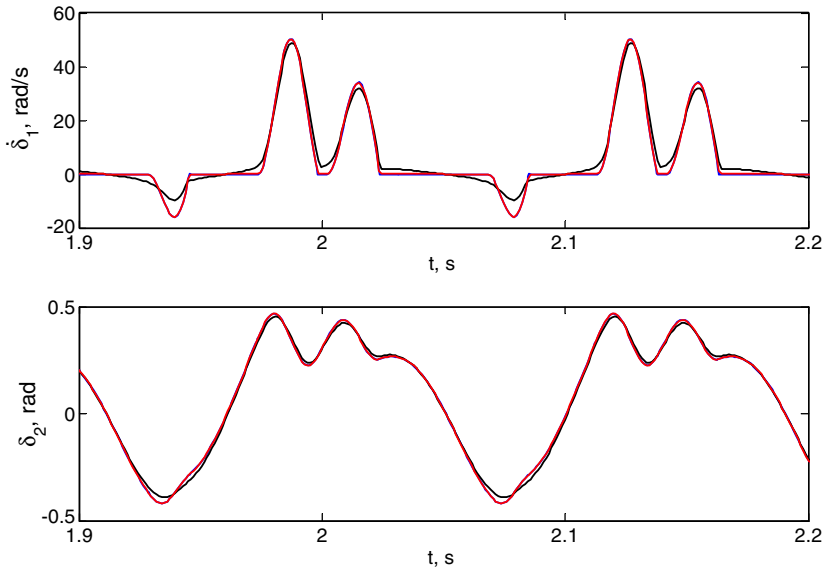

Fig. 6. Comparison of two friction path models in terms of time histories. ——, discontinuous friction model; - - - - - -, smoothened model with $\sigma = 0.5$; – - – - –, smoothened model with $\sigma = 10^2$.

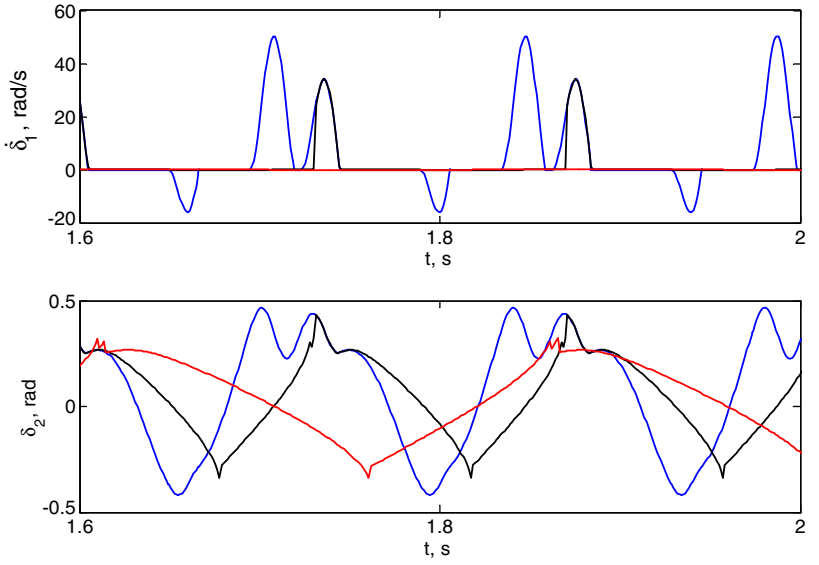

Fig. 7. Comparison of two friction path models in terms of time histories. ——, discontinuous model; - - - - - -, smoothened model with $\sigma = 10^3$; – - – - –, smoothened model with $\sigma = 2 \times 10^3$.

differences. On the other hand, when σ is 1000, the time domain responses of Fig. 7 are incorrect. Therefore, the dynamic response is very sensitive to the judicious choice of σ. Meanwhile, some almost periodic solutions may appear. These could be very misleading because the periodic solution is being sought, and a relative higher value of σ provides results that resemble the ones given by the discontinuous models. A comparison between the computational times clearly shows the advantage of a smoothened model. For instance, the calculations for $\dot{\delta}_1(t)$, etc. at one particular excitation frequency takes 15 s with the smoothened friction model with $\sigma = 100$ on a Pentium 4 1.7 GHz processor, while the discontinuous friction model consumes 50 s. However, as discussed earlier, the best value of σ usually is not known a priori and it could depend on system parameters. Consequently, the discontinuous friction model should be used as benchmark if successfully implemented. Further, our solution algorithm for discontinuous friction model could also be extended to other piecewise linear systems like the clearance nonlinearity. However, test or decision functions would need to be modified.

6. Effect of friction controlled path parameters

6.1. Bi-linear friction system analysis

Many researchers [2,3,5,6,8,11] have studied the conventional bi-linear friction system that assumes a massless link between the spring and the dry friction elements as shown in Fig. 8. Similar to the physical system of Fig. 3, equations for Fig. 8 can be given on a state by state basis. First, for the positive slip state, the equation is

$$\frac{I_1 I_3}{I_1 + I_3}\ddot{\delta}_1 + C\dot{\delta}_1 + T_{\mathrm{sf}} = \frac{I_3}{I_1 + I_3}T_e + \frac{I_1}{I_1 + I_3}T_D. \tag{32}$$

Since no inertial body exists between the dry friction and spring elements, the torque acting on the torsional spring is constant (T_{sf}). Consequently, the value of δ_2 remains T_{sf}/K and $\dot{\delta}_2$ is zero. Second, for the case of negative slip, the equation is rewritten as follows where $\delta_2 = -T_{\mathrm{sf}}/K$ and $\dot{\delta}_2 = 0$

$$\frac{I_1 I_3}{I_1 + I_3}\ddot{\delta}_1 + C\dot{\delta}_1 - T_{\mathrm{sf}} = \frac{I_3}{I_1 + I_3}T_e + \frac{I_1}{I_1 + I_3}T_D. \tag{33}$$

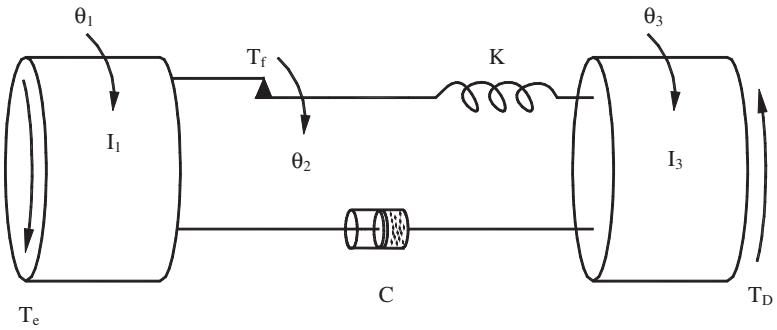

Fig. 8. Schematic of the bi-linear torsional system (with $I_2 \to 0$). Here, T_f represents a dry friction path.

Third, the equation for the pure stick state is given by

$$\frac{I_1 I_3}{I_1 + I_3}\ddot{\delta}_2 + C\dot{\delta}_2 + K\delta_2 = T_m + \frac{I_3}{I_1 + I_3}T_p(t). \tag{34}$$

As depicted in Figs. 4a and b, δ_1 remains constant and $\dot{\delta}_1$ is equal to zero. The integration procedure used here with the discontinuous friction model can now be applied to this system with a redefinition of the test $\Gamma(\tau)$ or decision $\mathrm{Re}(\tau)$ function:

$$\Gamma(\tau) = \mathrm{Re}(\tau) = K\delta_2. \tag{35}$$

The systems of Figs. 3 and 8 can now be compared. Both show the second-order system behavior under the pure stick condition. However, under the positive or negative slip state condition, the bi-linear friction system (of Fig. 8) exhibits a first-order system behavior while the model of Fig. 3 follows a second-order system. For this reason, some key differences between these two systems are expected, as explored in the subsequent section.

6.2. *Effect of the secondary inertia I_2*

A comparison of Eqs. (8) and (34) shows that the effect of the secondary (I_2) inertia could be negligible under the pure stick condition in the presence of a very small I_2. For this reason, we examine the effect of I_2 in the positive or negative slip state. First, consider a conventional bi-linear friction system undergoes transition from pure stick to positive slip state. Eq. (32) describes the governing equation for the system in the pure positive slipping motion. A phase term φ_c is intentionally included in the excitation torque expression since the absolute transition time t_c may not be integer multiplier of the excitation period (P). Consequently, given $T_D = T_m$, Eq. (32) has to be rewritten as follows where $I_{1e} = I_1 I_3/(I_1 + I_3)$ and $T_{pe} = T_p I_3/(I_1 + I_3)$.

$$I_{1e}\ddot{\delta}_1 + C\dot{\delta}_1 = (T_m - T_{\mathrm{sf}}) + T_{pe}\sin(\omega t + \varphi_c), \tag{36}$$

$$P = \frac{2\pi}{\omega}, \quad \varphi_c = \left[t_c - \mathrm{int}\left(\frac{t_c}{P}\right)\right]\omega. \tag{37a,b}$$

The operator int(·) yields the integer portion of a fraction number. Now, the general solution of $\dot{\delta}_1(t)$ is a combination of homogeneous and particular solutions as follows:

$$\dot{\delta}_1(t) = A\mathrm{e}^{-(C/I_{1e})t} + [a_0 + a_1\cos(\omega t) + a_2\sin(\omega t)]. \tag{38}$$

The coefficients (a_0, a_1 and a_2) are obtained by matching the particular solutions on both sides of Eq. (36) as follows:

$$a_0 = \frac{T_m - T_{\mathrm{sf}}}{C}, \quad a_1 = T_{pe}\frac{C\sin\varphi_c - I_{1e}\omega\cos\varphi_c}{I_{1e}^2\omega^2 + C^2}, \quad a_2 = T_{pe}\frac{C\cos\varphi_c + I_{1e}\omega\sin\varphi_c}{I_{1e}^2\omega^2 + C^2}. \tag{39a–c}$$

The constant A needs to be determined by the initial condition. As noted from the previous section, when the frictional interface experiences a transition from pure stick to positive slip motion, δ_2 reaches the maximum amplitude T_{sf}/K and retains this value during the entire subsequent pure slip state. To satisfy this dynamic condition, $\dot{\delta}_2$ experiences a finite jump from a

certain value V at the end of pure stick state to 0 at the start of pure slip state. For this reason, a corresponding finite jump from 0 to V must occur in $\dot{\delta}_1$ to satisfy the following continuity condition when we reset the transition time as 0.

$$(\dot{\theta}_1 - \dot{\theta}_3)|_{t=t_{0-}} = (\dot{\theta}_1 - \dot{\theta}_3)|_{t=t_{0+}}. \tag{40}$$

Thus, the initial condition of $\dot{\delta}_1(t)$ is determined, $\dot{\delta}_1(0) = V$. Use this to find A of Eq. (38) and write the complete response of $\dot{\delta}_1(t)$ as follows:

$$\dot{\delta}_1(t) = (V - a_0 - a_1)\mathrm{e}^{-(C/I_{1e})t} + a_0 + a_1\cos(\omega t) + a_2\sin(\omega t). \tag{41}$$

Observe that the oscillatory terms associated with a_1 and a_2 only contain only one frequency (ω).

Next, the 3dof system ($I_2 \neq 0$) is considered. Assume a very small I_2, say $I_2/I_1 = 0.005-0.01$. Eqs. (18) and (19) are approximated as follows:

$$I_2\ddot{\delta}_1 + C\frac{I_2}{I_1}(\dot{\delta}_1 + \dot{\delta}_2) - K\delta_2 + T_{\mathrm{sf}} = 0, \tag{42}$$

$$I_2\ddot{\delta}_2 + C\frac{I_2}{I_3}(\dot{\delta}_1 + \dot{\delta}_2) + K\delta_2 - T_{\mathrm{sf}} = 0. \tag{43}$$

Since the excitation torque is neglected due to $I_1 \gg I_2$, the phase lag φ_c term that accurately represent the excitation as discussed in the previous section is no longer an issue here. Further, Eq. (43) is further simplified given $I_3 \gg I_2$; refer to Table 1 for typical parameters.

$$I_2\ddot{\delta}_2 + C\frac{I_2}{I_3}\dot{\delta}_2 + K\delta_2 - T_{\mathrm{sf}} = 0. \tag{44}$$

Eq. (44) can be conveniently solved and the approximated solution for δ_2 is obtained where $\omega_n \cong \sqrt{K/I_2}$.

$$\delta_2(t) = b_0 + b_1\mathrm{e}^{-(C/2I_3)t}\cos(\omega_n t) + b_2\mathrm{e}^{-(C/2I_3)t}\sin(\omega_n t). \tag{45}$$

The initial conditions for $\delta_2(t)$ at the transition time are $\delta_2(0) = T_{\mathrm{sf}}/K$ and $\dot{\delta}_2(0) = V$. Since I_2 has a very small but non-zero value, its absolute velocity or momentum can only be changed by an infinite large impulsive force within an infinitesimal time span that is physically impossible. Consequently, no jump could take place in $\dot{\delta}_2(t)$ unlike the one exhibited by bi-linear friction system. Instead, $\dot{\delta}_2(t)$ is a smooth function of time.

$$\dot{\delta}_2(t) = \frac{T_{\mathrm{sf}}}{K} + \frac{V}{\omega_n}\,\mathrm{e}^{-(C/2I_3)t}\,\sin(\omega_n t). \tag{46}$$

As noted, $\delta_2(t)$ oscillates around the mean value T_{sf}/K unlike the bi-linear friction system. Further, since I_2 is very small, the oscillation frequency (ω_n) is very high. To conveniently obtain an approximate analytical solution for $\dot{\delta}_1(t)$, we neglect the damping term in Eq. (44) and substitute the relation in Eq. (42), and obtain the following governing equation:

$$I_2(\ddot{\delta}_1 + \ddot{\delta}_2) + C\frac{I_2}{I_1}(\dot{\delta}_1 + \dot{\delta}_2) = 0, \tag{47}$$

where the initial condition is defined as $(\dot{\delta}_1 + \dot{\delta}_2)|_{t=0} = \dot{\delta}_2|_{t=0} = V$. Finally, the approximate analytical solution of $\dot{\delta}_1(t)$ is obtained.

$$\dot{\delta}_1(t) = V[e^{-(C/I_1)t} - e^{-(C/2I_3)t}\cos(\omega_n t)]. \quad (48)$$

Similar to $\delta_2(t)$, a very high-frequency oscillatory term is found in $\dot{\delta}_1(t)$ along with an exponentially decaying term. Further, it is noted that the above analyses could be applied to the negative slip state in a similar manner.

Figs. 9 and 10 compare the results corresponding to $I_2/I_1 \neq 0$ (system of Fig. 3) and 0 (the conventional bi-linear system of Fig. 8) cases. As expected, the motion differences under the pure

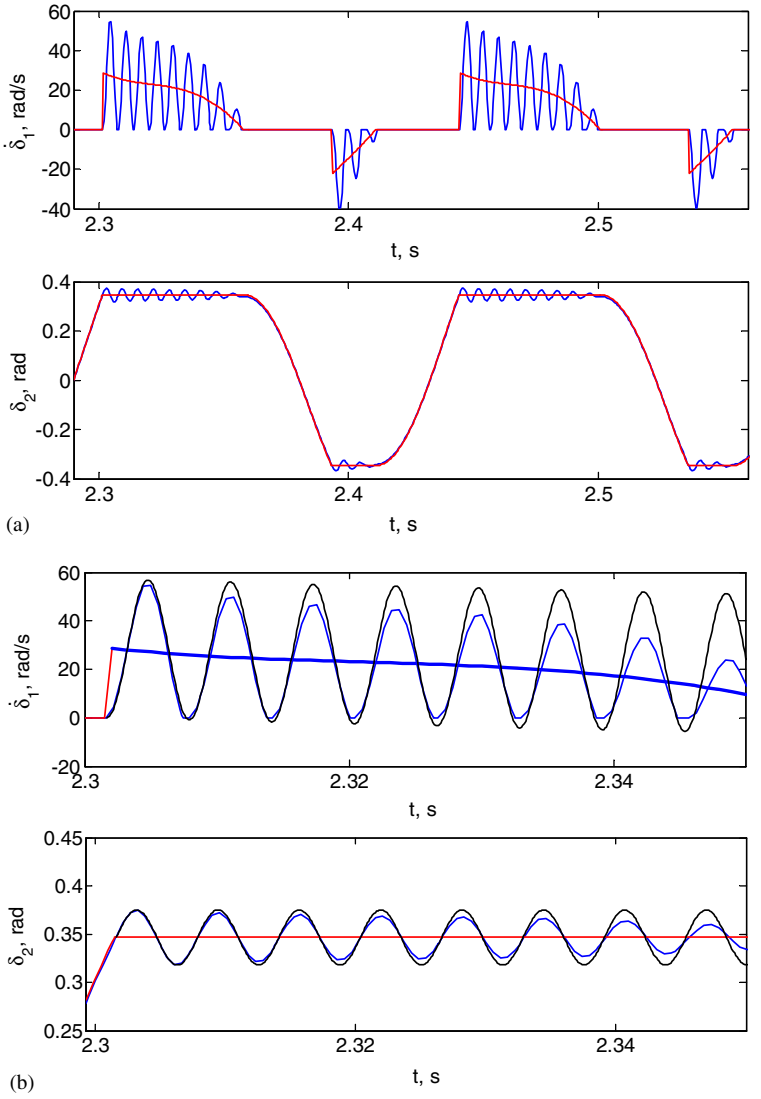

Fig. 9. Effect of I_2 on time histories: (a) numerical solutions: ——, $I_2/I_1 = 0$; - - - - - -, $I_2/I_1 = 0.005$; (b) comparison between numerical and analytical solution during the positive slip state: ——, numerical solution given $I_2/I_1 = 0$; . . . . ., analytical solution given $I_2/I_1 = 0$; - - - - -, numerical solution given $I_2/I_1 = 0.005$; – – – – – –, analytical solution given $I_2/I_1 = 0.005$.

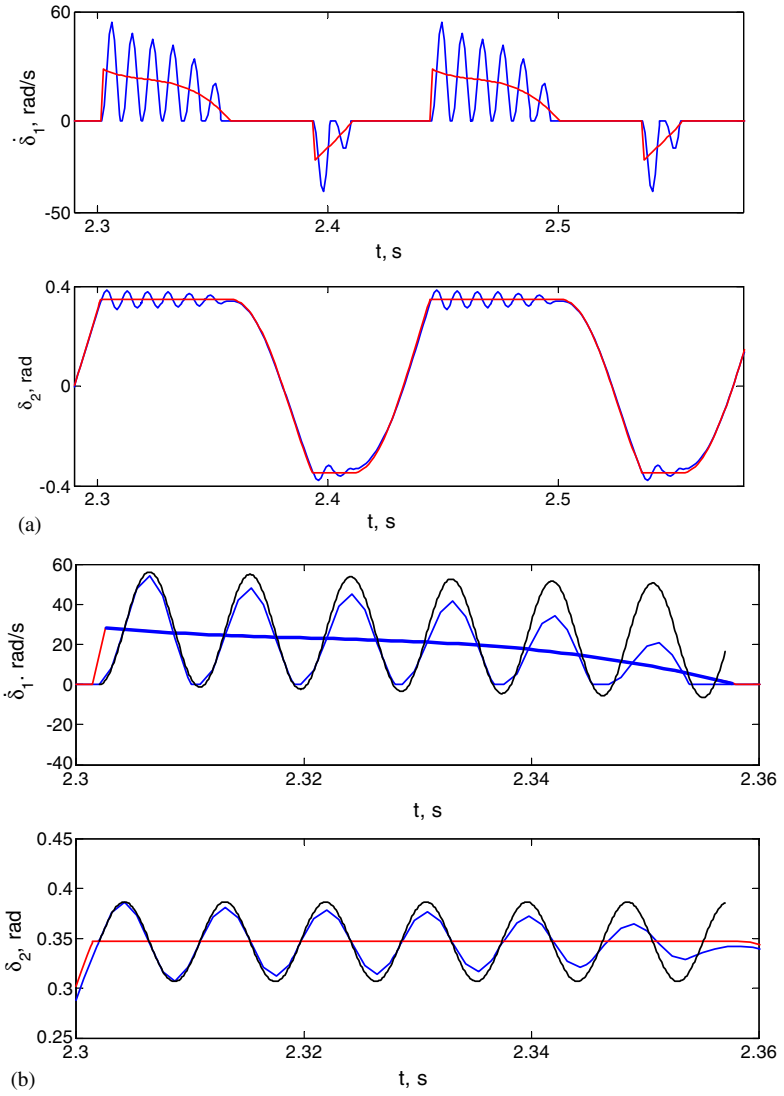

Fig. 10. Effect of I_2 on time histories: (a) numerical solutions: ——, $I_2/I_1 = 0$; - - - - - -, $I_2/I_1 = 0.01$; (b) comparison between numerical and analytical solution during the positive slip state: ——, numerical solution given $I_2/I_1 = 0$; . . . . ., analytical solution given $I_2/I_1 = 0$; - - - - - -, numerical solution given $I_2/I_1 = 0.01$; – — - – - –, analytical solution given $I_2/I_1 = 0.01$.

stick condition ($\dot{\delta}_1 = 0$) are minimal since I_2 is very small compared to I_1 as shown in Figs. 9a and 10a. Under the slip condition ($\dot{\delta}_1 > 0$), the difference is however noticeable. As response makes a transition from stick to slip, $\dot{\delta}_1$ of the bi-linear system (with $I_2 = 0$) shows a finite jump from zero to the value of $\dot{\delta}_2$ at the end of previous stick state and then it goes back to zero (stick) gradually. The values of δ_2 are bounded within $\pm T_{sf}/K$. Overall, the response resembles the "relaxation oscillation" [31], i.e. the potential energy is incrementally stored in the spring during the pure stick state and then suddenly released during the stick-to-slip transition. However, our response does

not quite follow the classical "relaxation oscillation" behavior since the underlying mechanism is essentially different. According to Den Hartog [32] and Andronov et al. [33], the "relaxation oscillation" is self-excited due to the existence of negative damping, such as the dry friction element with a negative slope in an autonomous system. In contrast, the response displayed by our bi-linear friction system is a result of the external torque excitation in the presence of a friction term and as such no negative damping element is present. In fact, Minorsky [34] has suggested that generic quasi-discontinuous motions may describe two kinds of oscillations: (i) relaxation oscillations and (ii) impulse-excited oscillations that are induced by an external impulsive cause. Although our response cannot be classified as impulse-excited oscillations either, we would still categorize as a quasi-discontinuous oscillations. Further research is needed to explore this issue.

On the contrary, the system response with a non-zero I_2 is, however, quite different. With the existence of a secondary inertia, an abrupt change or finite jump in $\dot{\delta}_1$ at the transition point does not occur. But the slip velocity is much higher than the one in the bi-linear friction case. With the initial conditions and absolute transition time provided by numerical solution, approximate analytical solutions for $\dot{\delta}_1$ and δ_2 are also obtained by using Eqs. (41), (46), and (48), respectively. Comparative results in Figs. 9b and 10b show a good agreement between the approximate analytical solutions and exact numerical solutions. Some minor difference for the $I_2 \neq 0$ case could be due to inadequate damping in the approximate model. The reason that $\dot{\delta}_1(t)$ just decreases gradually with time without active oscillations with bi-linear friction system is that the oscillatory term in Eq. (41) is at excitation frequency ω and this frequency is very low compared to $\omega_n = \sqrt{K/I_2}$ since a very small value of I_2 is used. Also, only period-one motions are observed.

Further, the response is investigated using phase-plane plots. As evident from Figs. 11a and c, the friction interface in the bi-linear hysteresis case always experiences two stops per cycle and the

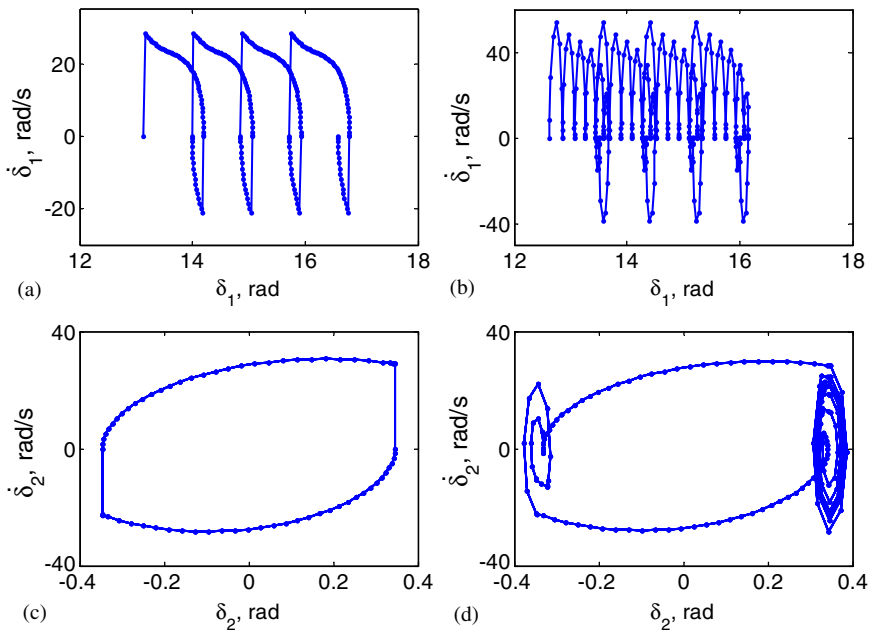

Fig. 11. Effect of I_2 on phase-plane plots: (a) and (c) are with $I_2/I_1 = 0$; (b) and (d) are with $I_2/I_1 = 0.01$.

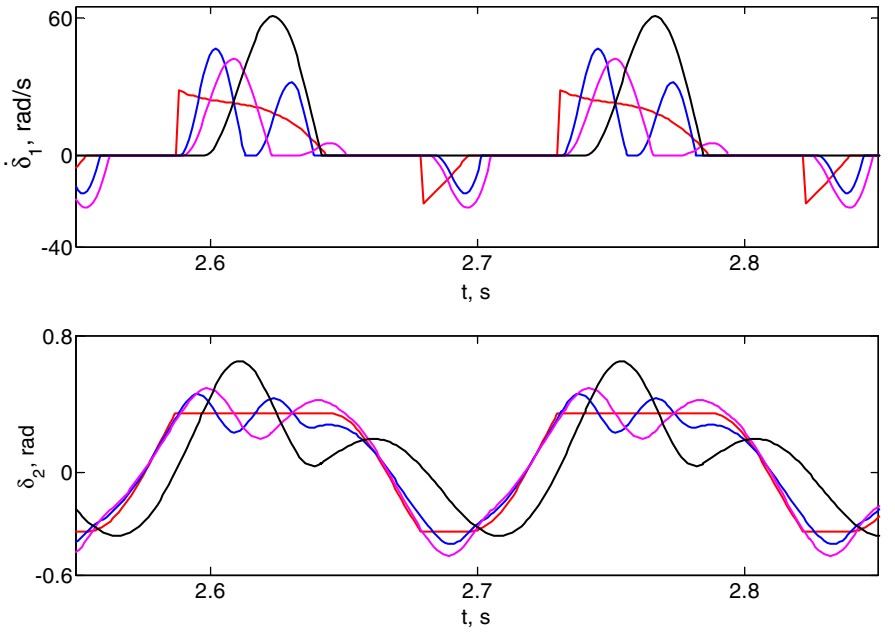

Fig. 12. Effect of I_2 on time histories: ——, $I_2/I_1 = 0$; - - - - - -, $I_2/I_1 = 0.1$; ....., $I_2/I_1 = 0.2$; – – – – –, $I_2/I_1 = 0.4$.

corresponding $\delta_2(t)$ shows a noticeable boundary at $\pm T_{sf}/K$. Compare the results of Fig. 11a and c ($I_2 = 0$) with Figs. 11b and d ($I_2 \neq 0$). More than 2 stops are experienced and $\delta_2(t)$ shows an oscillatory motion around $\pm T_{sf}/K$. The cusps formed in Figs. 11b and d are due to the stick–slip transitions.

More time histories plots are presented in Fig. 12. It is seen that an increase in I_2 decreases the severity of the interfacial stick–slip. At the excitation frequency of 7 Hz, the negative slip disappears when $I_2 = 0.4I_1$. As stated previously in the stick-to-slip boundary analysis, there exists a specific value of I_2 that would induce a purely stick regime and thus $\delta_2(t)$ is governed strictly by a linear system.

A more comprehensive understanding on the effect of I_2 could be achieved by constructing the nonlinear frequency response characteristics. Dynamic responses may be quantified by taking the maximum (max) and minimum (min) values from the calculated time history at each excitation frequency. Fig. 13a shows the response maps in terms of $\delta_{2\max}$ and $\delta_{2\min}$ values. Stick–slip boundaries as found earlier by the linear system theory are also plotted. Since there is no spring in parallel with the dry friction element, the relative displacement $\delta_1(t)$ may grow up to a very large value under the influence of a mean load T_m. Thus, no physical meaning could be associated with max or min values of the steady-state $\delta_1(t)$. Instead, the nonlinear frequency response of relative displacement δ_2 is of chief interest here. Also, we find the root-mean-square (rms) values from the calculated time histories, again at each excitation frequency as shown in Fig. 13b.

As expected from the stick-to-slip boundary analysis, an increase in the value of I_2 narrows the stick–slip regime. It is also clearly observed in Fig. 13a that as I_2 increases, the max-to-min value of δ_2 over the pure stick (linear) regime is lowered. However, the values over the stick–slip regime go up. Unlike the bi-linear hysteresis case where the peak amplitude is constant ($\delta_2 = T_{sf}/K$), the

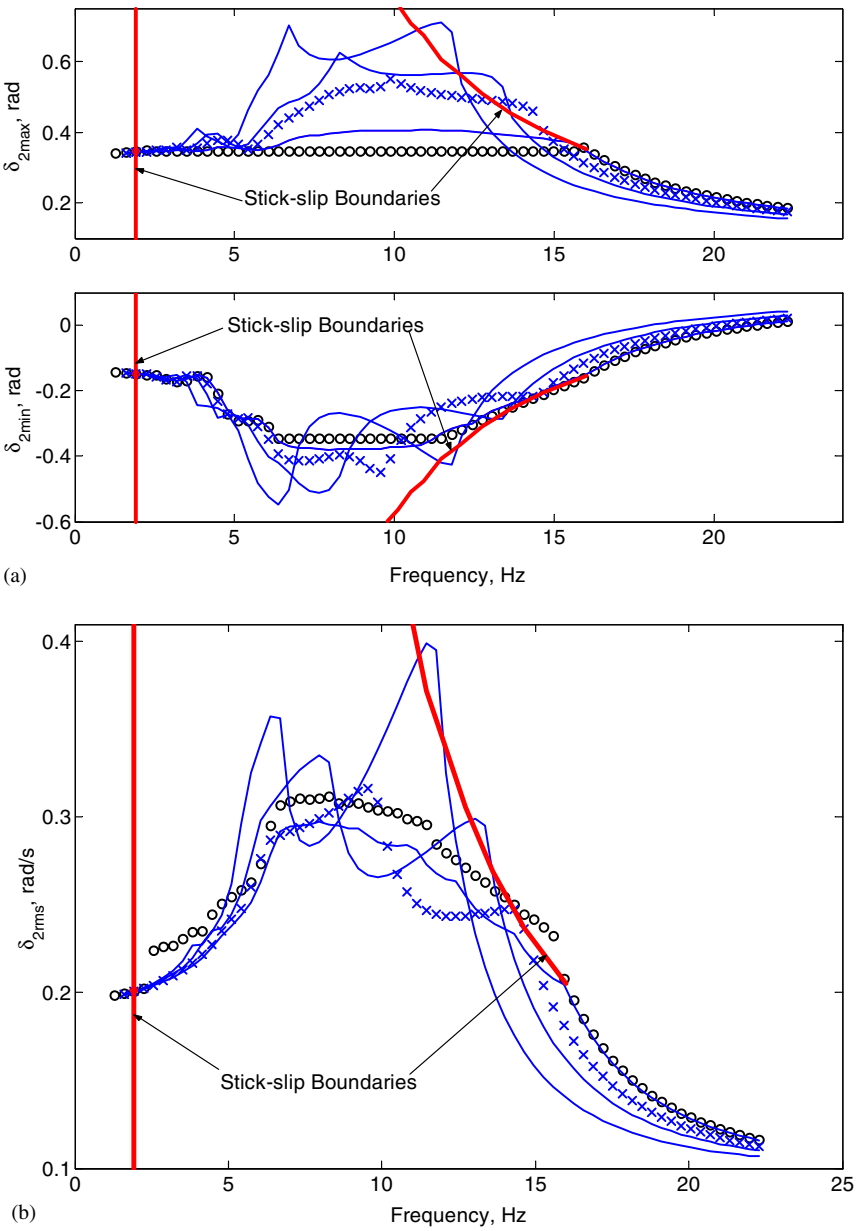

Fig. 13. Effect of I_2 on responses over a range of excitation frequencies: (a) maximum and minimum responses: ○, $I_2/I_1 = 0$; - - - - - -, $I_2/I_1 = 0.01$; ×, $I_2/I_1 = 0.1$; – - – - –, $I_2/I_1 = 0.2$; ——, $I_2/I_1 = 0.4$; (b) rms responses: ○, $I_2/I_1 = 0$; - - - - - -, $I_2/I_1 = 0.01$; ×, $I_2/I_1 = 0.1$; – - – - –, $I_2/I_1 = 0.2$; ——, $I_2/I_1 = 0.4$.

amplitudes with non-zero I_2 exhibit "resonance-like" curves in Fig. 13. Such resonances are dictated by a combination of 2 states: 2dof and 3dof system responses. A comparison of the rms maps in Fig. 13b shows similar effects of I_2.

6.3. Effect on the saturation friction torque T_{sf}

Fig. 14 shows the effect of T_{sf} on nonlinear frequency responses. As T_{sf} increases, the stick–slip regime narrows but the peak amplitude increases. Such a narrowing trend of the stick–slip regime is consistent with the stick-to-slip boundary analysis. Higher amplitudes of δ_2 can be explained by

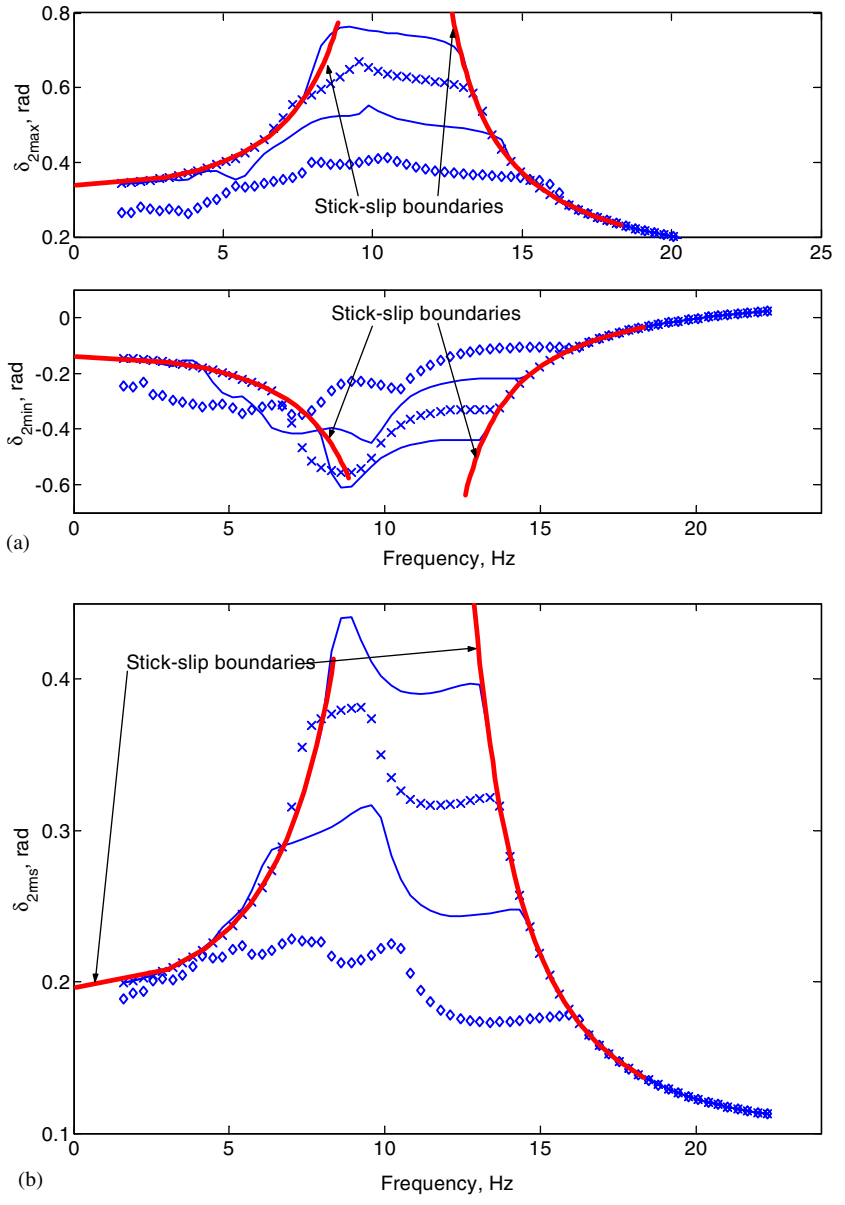

Fig. 14. Effect of T_{sf} on responses over a range of excitation frequencies: (a) maximum and minimum responses: ◇, $T_f = 250\,\mathrm{N\,m}$; - - - - - -, $T_f = 350\,\mathrm{N\,m}$; ×, $T_f = 450\,\mathrm{N\,m}$; ——, $T_f = 550\,\mathrm{N\,m}$; (b) rms responses: ◇, $T_f = 250\,\mathrm{N\,m}$; - - - - - -, $T_f = 350\,\mathrm{N\,m}$; ×, $T_f = 450\,\mathrm{N\,m}$; ——, $T_f = 550\,\mathrm{N\,m}$.

the fact that the sub-system of I_2 and I_3 now receives more excitation which is equal to T_{sf} under the slip condition. The severity of the stick–slip transition also decreases as evident from the time histories of Figs. 15a (at 10 Hz) and b (at 8 Hz). Fig. 15a shows that when T_{sf} is small such as 250 N m, 2 slips are found in each cycle. But when T_{sf} increases to 450 N m, the number of slips per cycle reduces to one. One could predict the trend of stick–slip regime as follows: T_{sf} first

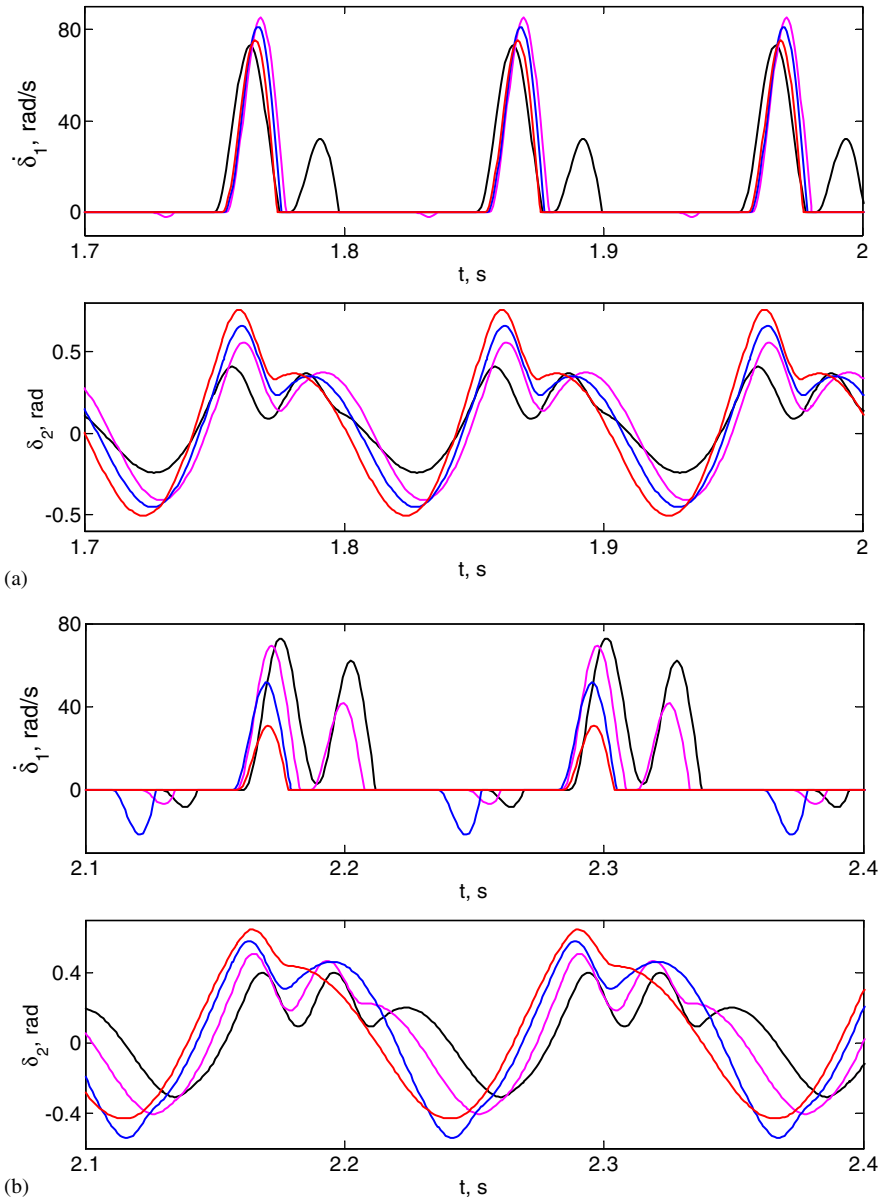

Fig. 15. Effect of T_{sf} on time histories: (a) excitation frequency is 10 Hz: - - - - - -, $T_f = 250$ N m; ....., $T_f = 350$ N m; – – – –, $T_f = 450$ N m; ——, $T_f = 550$ N m; (b) excitation frequency is 8 Hz: - - - - - -, $T_f = 250$ N m; ....., $T_f = 350$ N m; – – – –, $T_f = 450$ N m; ——, $T_f = 550$ N m.

reduces the slip velocity and its duration. Then the number of slips is reduced as T_{sf} is increased. Ultimately, this reduction would introduce the pure stick condition, i.e. non-slip or zero slip velocity.

7. Comparisons with benchmark studies

Next, we compare our method with two benchmark examples as available in the literature. These include Ferri and Heck's turbine blade damper study [15] and Hartung et al.'s passive vibration absorber analyses [26]. Physical models of both studies could be conceptually described by the sub-sets of Fig. 3 since the dry friction is the only nonlinear element in 2dof systems.

The model of Ferri and Heck's turbine blade damper is presented in Fig. 16a. The governing equations with dimensionless parameters (using the nomenclature of [15]) are as follows where y_1 and y_2 are the absolute displacements; $g(\dot{\mathsf{y}}_1)$ is the classical Coulomb friction force.

$$r\ddot{\mathsf{y}}_1 + p(\mathsf{y}_1 - \mathsf{y}_2) + g(\dot{\mathsf{y}}_1) = 0, \tag{49}$$

$$\ddot{\mathsf{y}}_2 + 2\varsigma\dot{\mathsf{y}}_2 + \mathsf{y}_2 + p(\mathsf{y}_2 - \mathsf{y}_1) = f\cos(\omega t). \tag{50}$$

Two example cases are selected to demonstrate the significant dynamic effect of the secondary mass (r). Our methods are applied to this system to first calculate the stick-to-slip boundaries, and then we conduct nonlinear simulations. Using both discontinuous and smoothened friction torque models of earlier sections, we predict frequency responses that match quite well with Ferri and Heck's results in Figs. 17 and 18. A minor difference is seen around $\omega = 0.94$ in Fig. 17a when σ is

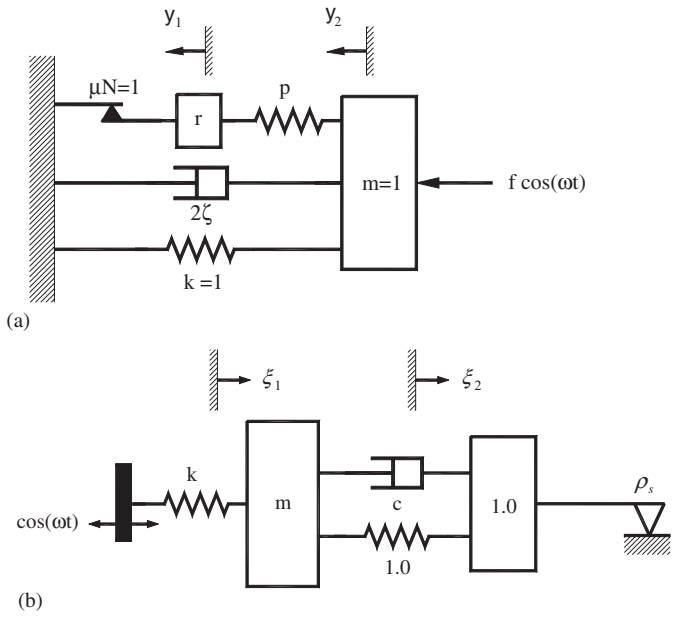

Fig. 16. Benchmark models with dry friction element: (a) Ferri and Heck's turbine blade friction damper model [15] and (b) Harung et al.'s passive vibration absorber model [26].

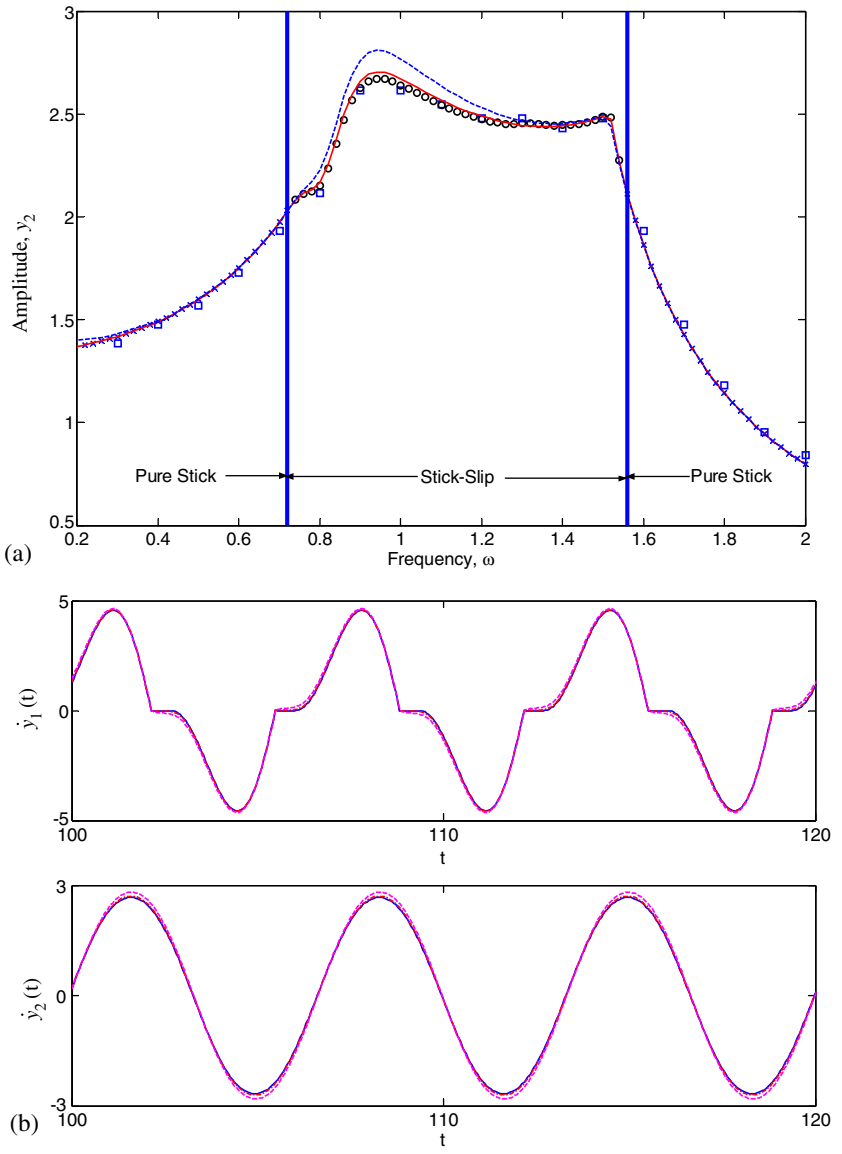

Fig. 17. Comparison with Ferri and Heck's results: (a) frequency response curves with $f = 2$, $p = 0.5$ and $r = 0.2$. ×, pure stick solution; ○, discontinuous friction model; ——, smoothened friction model with $\sigma = 50$; - - - - - -, smoothened friction model with $\sigma = 10$; □, Ferri and Heck's results. (b) Time histories at $\omega = 0.94$: ——, discontinuous friction model; - - - - - -, smoothened friction model with $\sigma = 10$; – - - - –, smoothened friction model with $\sigma = 50$.

changed from 50 to 10. However, as shown by the time history in Fig. 17b, this difference is within 5%. Further, our results generate more insight into the system by analytically pinpointing the pure stick (linear) and stick–slip (nonlinear) frequency regimes.

Hartung et al. [26] studied the dynamics of a 2dof system (vibration absorber) as shown in Fig. 16b. The governing equations are as follows using their nomenclature.

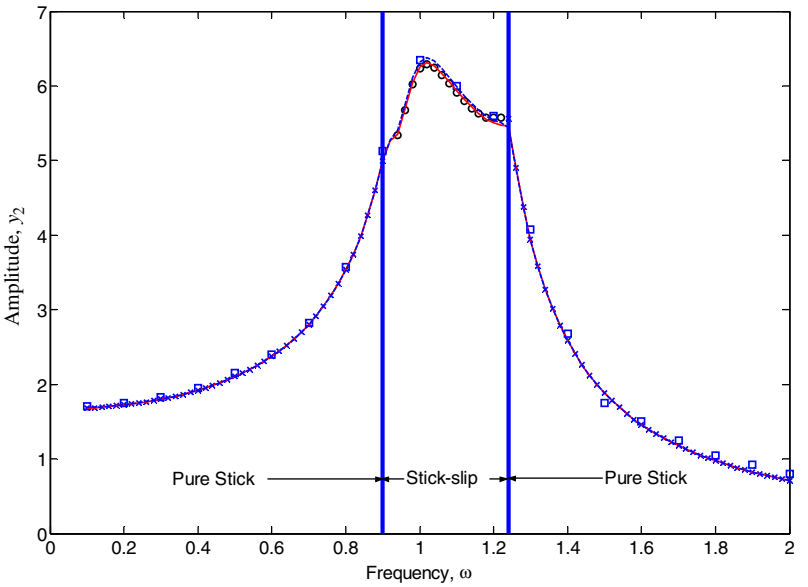

Fig. 18. Frequency response curves with $f = 2$, $p = 0.2$ and $r = 0.05$. ×, pure stick solution; ○, discontinuous friction model; ——, smoothened friction model with $\sigma = 50$; - - - - - -, smoothened friction model with $\sigma = 10$; □, Ferri and Heck's results.

$$m\dot{\xi}_1 + c\dot{\xi}_1 - c\dot{\xi}_2 + (1+k)\xi_1 - \xi_2 = k\cos(\omega t), \tag{51}$$

$$\dot{\xi}_2 - c\dot{\xi}_1 + c\dot{\xi}_2 - \xi_1 + \xi_2 = -\rho_s g(\dot{\xi}_2). \tag{52}$$

Aside from numerical simulation based on the discontinuous friction model, they also conducted an experimental study and investigated the effect of friction force amplitude ρ_s. Selected measured frequency response curves under three friction forces are extracted from Ref. [26] and illustrated in Fig. 19. First, we predict the stick-to-slip boundaries using the linear system procedure proposed earlier. Second, we employ the discontinuous and smoothened friction models. Our simulation results, as shown in Fig. 20, show a very good match with measured curve of Fig. 19 even when the smoothened friction model is chosen. As the friction force increases, the stick–slip motion is suppressed in Fig. 20. The stick–slip motion virtually disappears in Fig. 20c when the friction force increases to a certain value and finally the system is degenerated into a linear sdof system. Although, Hartung et al.'s experiment [26] showed that the friction-induced characteristics depend on normal or friction force amplitude, our comparisons reveal that the even simplest friction model could still be used to qualitatively assess the nonlinear responses or quantitatively estimate the stick–slip boundaries. Thus, we validate our linear and nonlinear methods.

8. Conclusion

Unlike previous studies that focused on the frictional interface models, we have examined the nonlinear time and frequency domain responses of a 3dof system subjected to localized stick–slip

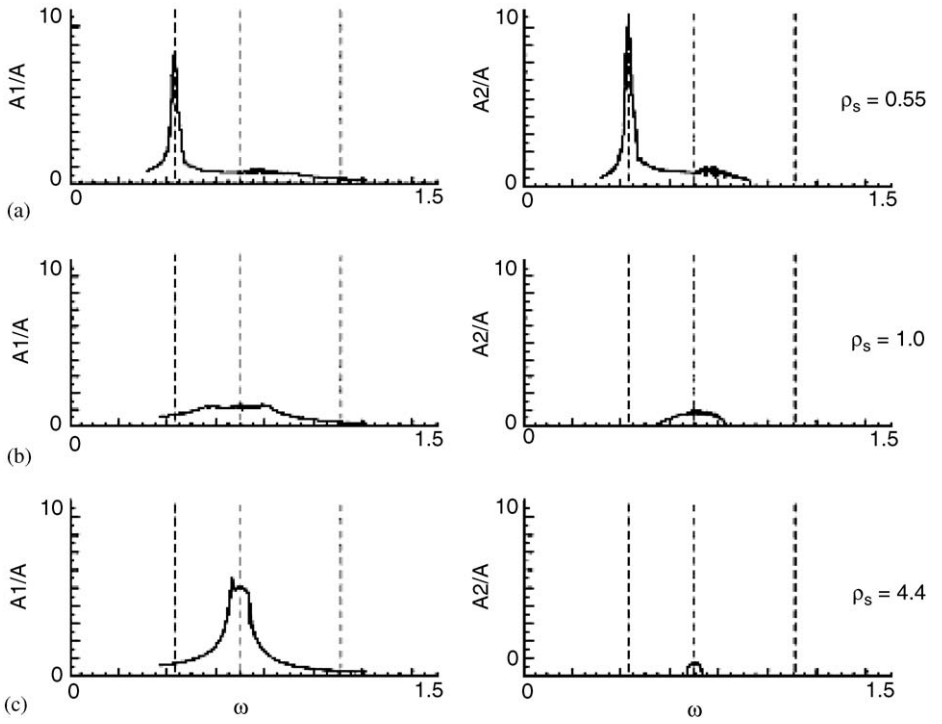

Fig. 19. Measured frequency response curves (Hartung et al.'s experiment scanned from Ref. [26]).

motions. Three contributions emerge. First, a procedure to calculate the stick-to-slip boundaries has been developed based on the linear system theory. This procedure yields reliable prediction of the thresholds and thus it can quickly identify linear or nonlinear frequency regimes. Second, both smoothened and discontinuous friction models are studied and compared with each other. A direct time domain numerical integration can be employed to solve the smoothened friction model and it speeds up the calculation. Though a judicious choice of the conditioning factor can generate reasonably close solutions, one must exercise caution in using the smoothening procedure without some prior knowledge of the system. Third, the effect of the secondary inertia is investigated in depth using both time and frequency domain calculations. Both approximate analytical and numerical solutions clearly illustrate that even a very small secondary inertia has a significant influence on the behavior and thus the bi-linear friction system (such as Fig. 8) must be used with caution. During the slip states, $\dot{\delta}_1(t)$ follows a first-order behavior when $I_2 = 0$ and a second-order system when $I_2 \neq 0$. As evident from time histories and frequency responses, the amplitudes of $\delta_2(t)$ are bounded for a bi-linear system and its frequency responses form a flat top. But when $I_2 \neq 0$, no specific bounds can be defined for $\delta_2(t)$ and its frequency responses show resonance-like curves. These resonances are essentially determined by a combination of 2 states: 2dof and 3dof nonlinear system responses.

The frictional interface dynamics and the response of the overall system is dictated by the secondary inertia I_2. At a higher value of I_2, the stick–slip phenomena are suppressed. However,

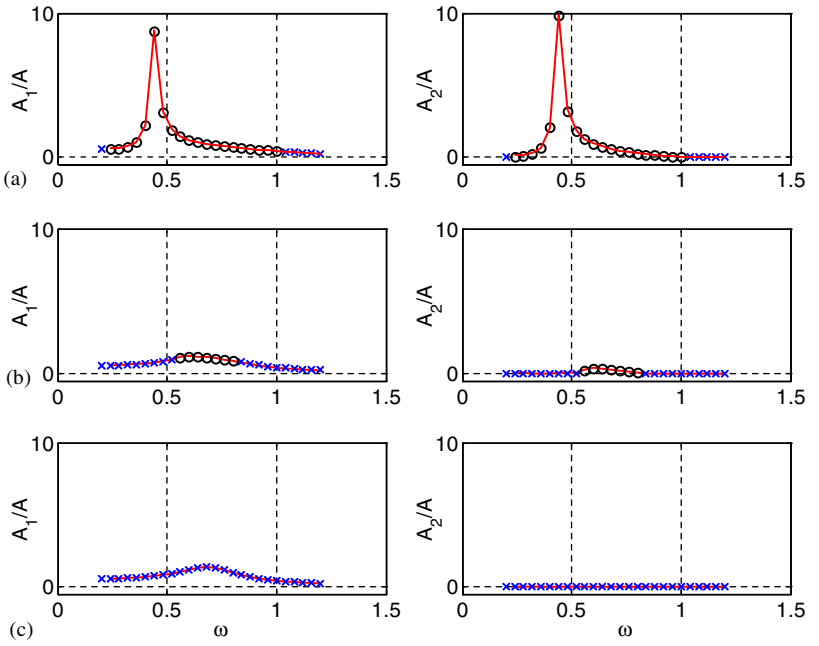

Fig. 20. Simulated frequency response curves. ×, pure stick solution; ○, discontinuous model (stick–slip) solution; ——, smoothened friction model with $\sigma = 50$.

the peak amplitudes of the response could still go up. Similar effect is observed by a change in the saturation friction torque. Although, the system response is strongly nonlinear, the suppression of stick–slip phenomena seems to the follow the following pattern: first reduce the slip velocity and then reduce the number of slips.

The advantage of our smoothened and discontinuous friction models is limited to a system of low dimension. As the system dimension increases, time domain simulations could become very cumbersome since many nonlinear functions must be evaluated. Conceptually, semi-analytical techniques need to be developed. Effects along this direction are reported in a subsequent article [35].

Acknowledgements

Research support from the DaimlerChrysler Challenge Fund is gratefully acknowledged.

References

[1] K. Brack, *Beschreibung und Implementierung des übertragungsverhaltens von hydrodynamischen Drehmomentwandlern in MSC/NASTRAN*, Diplomarbeit, Universität Kaiserslautern, 1996.

[2] R. Fischer, D. Otto, Torque converter clutch systems, *the Fifth Luk Symposium*, May 1994, pp. 107–138.

[3] P. Attibele, DaimlerChrysler powertrain engineer, Personal Communications, April 2002.
[4] D. Karnopp, Computer simulation of stick–slip friction in mechanical dynamic systems, *Journal of Dynamic Systems, Measurement, and Control* 107 (1985) 100–103.
[5] W.D. Iwan, A distributed-element model for hysteresis and its steady-state dynamic response, *Journal of Applied Mechanics* 33 (1966) 893–900.
[6] C.H. Menq, J. Bielak, J.H. Griffin, The influence of microslip on vibratory response, Part I: a new microslip model, *Journal of Sound and Vibration* 107 (2) (1986) 279–293.
[7] T. Imamura, O. Sato, K. Sano, K. Tomioka, Development of shift control for a 5-speed AT using Matlab, *JATCO Technical Review*, No. 3, June 2002, pp. 31–37.
[8] J.P. Den Hartog, Forced vibrations with combined coulomb and viscous friction, *Transactions of the ASME* APM-53-9 (1931) 107–115.
[9] T.K. Pratt, R. Williams, Nonlinear analysis of stick/slip motion, *Journal of Sound and Vibration* 74 (4) (1981) 531–542.
[10] S.W. Shaw, On the dynamic response of a system with dry friction, *Journal of Sound and Vibration* 108 (2) (1986) 305–325.
[11] C.H. Menq, J.H. Griffin, J. Bielak, The forced response of shrouded fan stages, *Journal of Vibration, Acoustics, Stress, and Reliability in Design* 108/51 (1986) 50–55.
[12] C.H. Menq, B.D. Yang, Non-linear spring resistance and friction damping of frictional constraint having two-dimensional motion, *Journal of Sound and Vibration* 217 (1) (1998) 127–143.
[13] J.H. Wang, W.K. Chen, Investigation of the vibration of a blade with friction damper by HBM, *Journal of Engineering for Gas Turbines and Power* 115/295 (1993) 294–299.
[14] J.H. Wang, Design of a friction damper to control vibration of turbine blades, in: A. Guran, F. Pfeiffer, K. Popp (Eds.), *Dynamics with Friction Modeling Analysis and Experiment*, 1996, pp. 169–195.
[15] A.A. Ferri, B.S. Heck, Vibration analysis of dry friction damped turbine blades using singular perturbation theory, *Nonlinear and Stochastic Dynamics*, *ASME*, 1994, AMD-Vol. 192/DE-Vol. 78, pp. 47–56.
[16] A.A. Ferri, Friction damping and isolation systems, *Transactions of the ASME* 117 (1995) 196–206 (Special 50th Anniversary Design Issue).
[17] B.L. Van De Vrande, D.H. Van Campen, A. De Kraker, An approximate analysis of dry-friction-induced stick–slip vibration by a smoothing procedure, *Nonlinear Dynamics* 19 (1999) 157–169.
[18] R.L. Leine, D.H. Van Campen, A. De Kraker, Stick–slip vibrations by alternate friction models, *Nonlinear Dynamics* 16 (1) (1998) 41–54.
[19] E.J. Berger, M.R. Begley, M. Mahajani, Structural dynamic effects on interface response: formulation and simulation under partial slipping conditions, *Journal of Applied Mechanics* 67 (2000) 785–792.
[20] E.J. Berger, C.M. Krousgrill, On friction damping modeling using bilinear hysteresis elements, *Journal of Vibration and Acoustics* 124 (2002) 367–375.
[21] C. Padmanabhan, R. Singh, Dynamics of a piecewise non-linear system subject to dual harmonic excitation using parametric continuation, *Journal of Sound and Vibration* 184 (5) (1995) 767–799.
[22] N. Yamada, K. Ando, An analysis of clutch self-excited vibration in automotive drive line, SAE Paper 951319.
[23] R. Singh, H. Xie, R.J. Comparin, Analysis of automotive neutral gear rattle, *Journal of Sound and Vibration* 131 (2) (1989) 177–196.
[24] T.C. Kim, T.E. Rook, R. Singh, Super- and sub-harmonic response calculations for a torsional system with clearance non-linearity using the harmonic balance method, *Journal of Sound and Vibration* 281 (3–5) (2005) 965–993.
[25] R.J. Comparin, R. Singh, Non-linear frequency response characteristics of an impact pair, *Journal of Sound and Vibration* 134 (2) (1989) 259–290.
[26] A. Hartung, H. Schmieg, P. Vielsack, Passive vibration absorber with dry friction, *Archive of Applied Mechanics* 71 (2001) 463–472.
[27] T.C. Kim, T.E. Rook, R. Singh, Effect of smoothening functions on the frequency response of an oscillator with clearance non-linearity, *Journal of Sound and Vibration* 263 (2003) 665–678.
[28] J.R. Dormand, P.J. Prince, A family of embedded Runge–Kutta formulae, *Journal of Computational and Applied Mathematics* 6 (1) (1980) 19–26.

[29] C.W. Gear, O. Osterby, Solving ordinary differential equations with discontinuities, *ACM Transactions on Mathematical Software* 10 (1) (1984) 23–44.
[30] C. Padmanabhan, R.C. Barlow, T.E. Rook, R. Singh, Computational issues associated with gear rattle analysis, *Journal of Mechanical Design* 117 (1995) 185–192.
[31] A.H. Nayfeh, D.T. Mook, *Nonlinear Oscillations*, Wiley, New York, 1995.
[32] J.P. Den Hartog, *Mechanical Vibrations*, Dover Publications, New York, 1985.
[33] A.A. Andronov, A.A. Vitt, S.E. Khaikin, *Theory of Oscillators*, Dover Publications, New York, 1987.
[34] N. Minorsky, *Non-linear Mechanics*, J.W. Edwards, 1947.
[35] C. Duan, R. Singh, Super-harmonics in a torsional system with dry friction path subject to harmonic excitation under a mean torque, *Journal of Sound and Vibration*, in press; doi:10.1016/j.jsv.2004.08.020.